YU ISSN 0015—3206
FZKAAA 22 (1) 183 (1990)

STRUCTURE OF THE LOW-LYING NUCLEAR STATES OF ^{101}Mo

HELMUTH SEYFARTH, HASAN H. GÜVEN+, BELA KARDON++, GÉRARD LHERSONNEAU+++, KORNEL SISTEMICH and SLOBODAN BRANT*

Institut für Kernphysik, Kernforschungsanlage Jülich, 5170 Jülich, F. R. Germany

NORBERT KAFFRELL

Institut für Kernchemie, Johannes Gutenberg-Universität Mainz, 6500 Mainz, F. R. Germany

PETER MAIER-KOMOR

Physik-Department, Technische Universität München, 8046 Garching, F. R. Germany

HELBERT K. VONACH

Institut für Radiumforschung und Kernphysik der Universität Wien, 1090 Wien, Austria

VLADIMIR PAAR** and DRAŽEN VORKAPIĆ**

Prirodoslovno-matematički fakultet, University of Zagreb, 41000 Zagreb, Yugoslavia

RICHARD A. MEYER

Nuclear Physics Division, U. S. Department of Energy, Washington D. C. 20545

and Lawrence Livermore National Laboratory, Livermore, California 94550, USA

Received 9 October 1989

UDC 539.14

Original scientific paper

Excited states of ^{101}Mo with energies up to 1447 keV have been studied through spectroscopy of the γ radiation following thermal neutron capture in ^{100}Mo and β^- decay of ^{101}Nb. From proton angular distributions, measured in the

+ Present address: Istanbul Technical Univeristy, Maslak/Istanbul, Turkey.

++ Present address: Hungarian Academy of Sciences, Central Research Institute for Physics, Budapest, Hungary.

+++ Present address: Institut für Kernchemie, Johannes Gutenberg-Universität Mainz.

* Alexander von Humboldt fellow 1987/1988, on leave of absence from University of Zagreb, 41000 Zagreb, Yugoslavia.

** Supported by Internationales Büro, Kernforschungsanlage Jülich.

^{100}Md (d, p) reaction with 14 MeV deuteron energy, angular momentum-transfer values have been deduced for states with $E_{ex} \leq 583$ keV. Several new states have been established and existing discrepancies between the results of earlier investigations have been removed. IBFM/PTQM calculations, taking into consideration the transitional character of the ^{100}Mo boson core, have been performed to study the structure of the positive parity states with $E_{ex} < 600$ keV and their electromagnetic properties.

1. Introduction

The nucleus $^{101}_{42}Mo_{59}$ is situated at the onset of the region of deformation around mass number $A = 100$. It is well known that the $N = 58$ isotones like ^{96}Sr, ^{97}Y and ^{98}Zr have non-rotational character at low excitation energy. Contrary to this behaviour evidence for ground-state deformation has been observed for the $N = 60$ isotones ^{97}Rb through ^{101}Nb. Shape coexistence seems to occur in the $N = 59$ isotonic chain to which ^{101}Mo belongs. Thus it has been shown[1] that the ground-state of ^{97}Sr is based on the $s_{1/2}$ neutron orbit in accordance with the shell model for spherical nuclei while a rotational band is built upon the 585 keV excited state[2,3]. For the odd-odd nucleus ^{98}Y in this isotonic chain the existing data and calculations in the framework of the interacting boson fermion-fermion model (IBFFM) indicate coexistence of spherical and higher-lying deformed states, too[3]. On the other hand, in the Mo isotopic chain ^{101}Mo is situated between ^{99}Mo, the low-lying states of which[4] are well described by the quasiparticle-phonon coupling model[5], and ^{103}Mo which has a rotational ground-state band[6]. The transitional character and the question, whether coexisting structures show up in ^{101}Mo, challenge a detailed experimental and theoretical study of this nucleus.

A variety of ealier experimental studies on the level scheme have been performed[7-9]. These investigations of the γ radiation following thermal and resonance neutron capture in ^{100}Mo and the β^- decay of ^{101}Nb, and of the ^{100}Mo (d, p) and ^{100}Mo (t, d) neutron stripping reactions using polarized and unpolarized deuteron and triton beams have resulted in a detailed level scheme for excitation energies ≤ 1 MeV. However, a number of discrepancies among the experimental results emerged. The present study on the γ radiation following thermal neutron capture in ^{100}Mo and the β^- decay of ^{101}Nb succeeds in disentangling most of these problems. Preliminary results of the present studies of thermal neutron capture[7,10], β^- decay of ^{101}Nb[11,12] and of the (d, p) reaction[13] have been published already. New experimental data on the first excited $J^\pi = 3/2^+$ state at 13.5 keV and the second excited $5/2^+$ state at 57.0 keV (half-lives, decay modes) have been obtained from the present experiments. These results are published elsewhere[14].

Recently, IBFM calculations for odd-even nuclei[15,16] and IBFFM calculations for odd-odd nuclei[16,17] in the region around $A = 100$ have been performed successfully. Therefore, the IBF model in the equivalent representation of the particle-truncated quadrupole-phonon coupling model (PTQM) has now been applied to ^{101}Mo in order to get more insight into the structure of the low-lying states ($E_{ex} < 600$ keV). A detailed discussion of the triplet of $1/2^+$ ground-state, 13.5 keV $3/2^+$ state, and 57.0 keV $5/2^+$ state[14] shows that the $3/2^+$ state

is of $(d_{5/2})^3_{3/2} j - 1$ type, whereas the ground-state and the 57.0 keV state mainly have single quasi-particle character. The present paper extends the interpretation in the framework of IBFM/PTQM to states of higher excitation energy.

2. *Experimental methods and results*

2.1. β^- *decay of* ^{101}Nb

At the fission-product separator LOHENGRIN[18] installed at the HFR of the ILL Grenoble, the mass chain $A = 101$ was investigated by γ-ray singles (including multispectrum analysis) and γ-γ coincidence measurements using 32 and 70 cm^3 Ge (Li) detectors (energy resolution: 0.75 keV at 122 keV and 2.0 keV at 1333 keV, respectively). The experiments were performed with the separator set for the ratio of the mass and the ionic charge of the fission products to $A/q = 101/21$ and a contamination of the mass chain 96 ($A/q = 96/20$) was observed. The low-energy part of the γ-ray spectrum taken with the 32 cm^3 detector is shown in Fig. 1. The energies and intensities of the γ-rays assigned to the decay of ^{101}Nb and the measured γ-γ coincidence relationships are given in Section 3 together with the data from the ^{100}Mo (n, γ) study.

2.2. *Thermal neutron capture in* ^{100}Mo

With metallic Mo powder, enriched in ^{100}Mo (Table 1), γ-ray spectra following thermal neutron capture have been measured at the external beam facility[20] at the FRJ-2 research reactor (DIDO) of KFA Jülich. Various detectors and targets have been used to cover the range from the low-energy secondary to the high-energy primary transitions. For $10 \leq E_\gamma \leq 250$ keV two targets with effective thicknesses of 37 and 162 mg/cm^2 were used. They were suspended at an angle of 30° to the axis of the vertical neutron beam within the neutron shielding tube in front of a 1.4 cm^3 HPGe detector. Details of the set-up and the relative detection

TABLE 1.

mass no.	abundance[a] /at. %	σ_{th}[b]/barn	thermal capture contribution/%
92	0.60(2)	0.019	0.044
94	0.23(2)	0.015	0.013
95	0.40(2)	14.0(5)	21.5(13)
96	0.81(2)	0.5(2)	1.6(6)
97	0.36(2)	2.1(5)	2.9(7)
98	1.69(5)	0.130(6)	0.84(5)
100	95.9(1)	0.199(3)	73.2(11)

[a] analysis of the manufacturer Union Carbide Corp., ORNL, Tennessee, USA.

[b] from Ref. 19.

1 barn = 10^{-24} cm^2

Isotopic composition and thermal neutron capture contribution of the target material used in the present measurements.

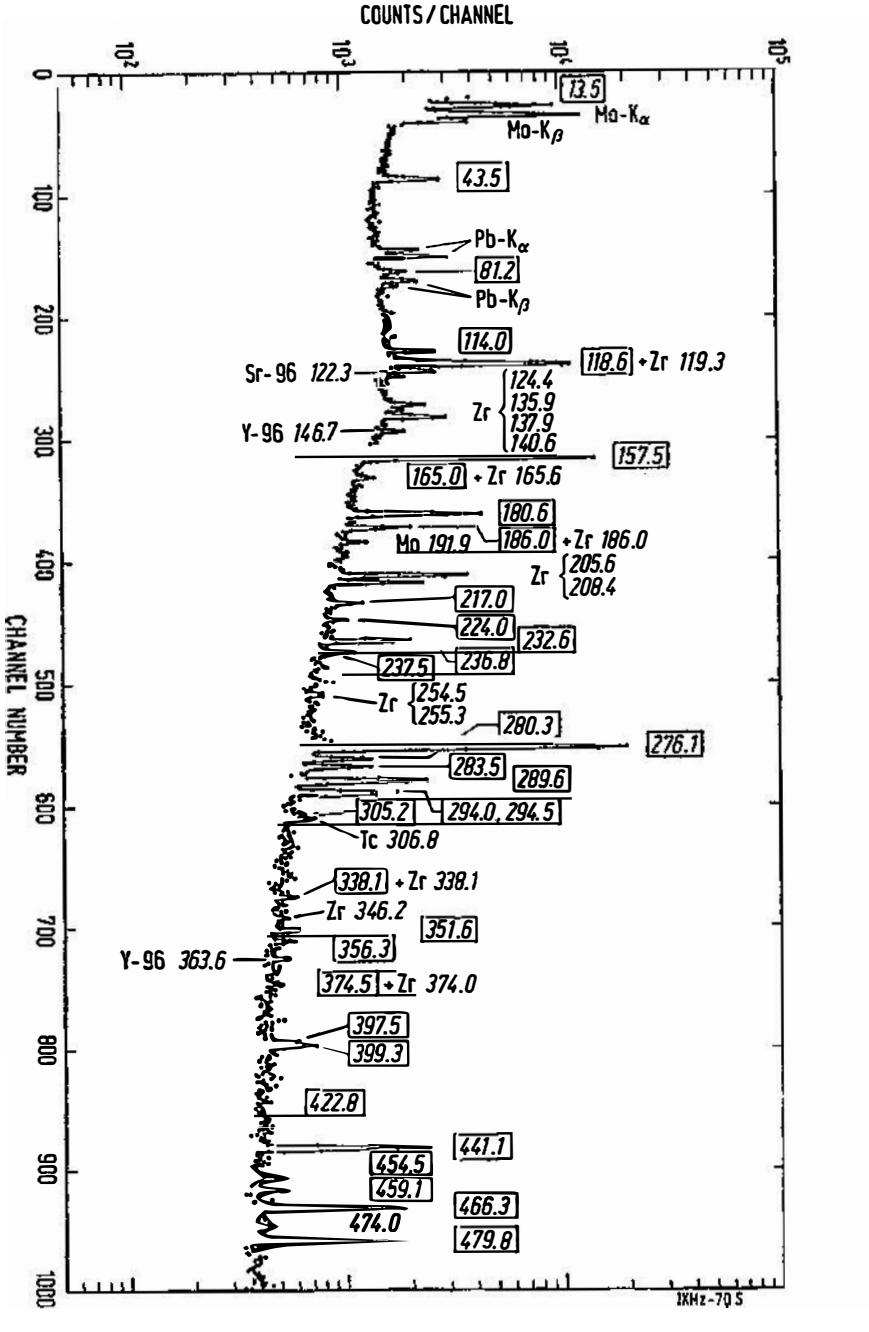

Fig. 1. Low-energy part of the γ-ray spectrum from ^{101}Nb β^--decay measured with the 32 cm^3 detector at LOHENGRIN. The energies of the γ-rays assigned to the decay of ^{101}Nb are given in boxes.

efficiency have been given elsewhere[21]. As an example, Fig. 2 shows a spectrum recorded with the 162 mg/cm^2 target. The small thermal neutron capture cross section of ^{100}Mo and the small quantity of target material result in a low target capture rate. Thus, in the spectrum lines from neutron capture in the Ge detector material[22] and the Al cryostat[23] show up which by part are superimposed on Mo lines (upper part of Fig. 2). Therefore, a spectrum measured with empty target holder was subtracted from this spectrum after normalization to equal measuring times. The resulting spectrum (lower part of Fig. 2) e. g. yields the low-energy ^{101}Mo line of 13.5 keV. The spectrum for $E_\gamma \leq 1500$ keV was investigated with the use of a 5.8 cm^3 planar and a 38 cm^3 true coaxial Ge (Li) detector[24] and thicker targets. The energy and relative efficiency calibrations were performed with ^{241}Am, ^{57}Co, ^{133}Ba and ^{152}Eu radioactive sources[25] placed at the position of the Mo target.

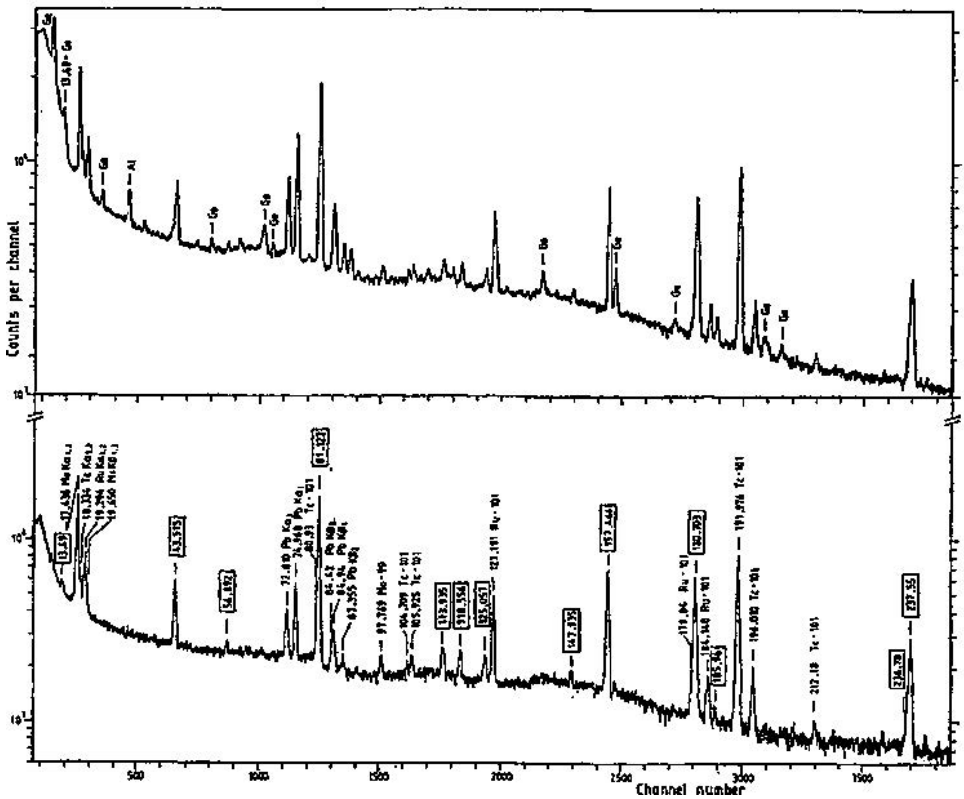

Fig. 2. Low-energy neutron-capture γ-ray spectrum measured with the 162 mg/cm^2 Mo target (upper part) and the spectrum which results from subtraction of the background spectrum measured with empty target holder. The peaks are labelled by the γ-ray energies resulting from fit and correction for non-linearity of the electronic system. Energies of lines from the ^{100}Mo (n, γ) reaction are given in boxes. The errors of the ^{101}Tc and ^{101}Ru energies are ≤ 25 eV, those of the X-rays ≤ 10 eV.

The high-energy γ-ray spectrum was measured with the 38 cm^3 true coaxial Ge (Li) detector and a 10 cm^3 rectangular Ge (Li) detector of 0.5 cm depletion depth. The two detectors have different double-escape peak (DEP) and single-escape peak (SEP) to full energy peak (FEP) ratios. Therefore, the comparison of spectra taken with both detectors facilitates the identification of the γ-ray lines in the complex spectrum (Fig. 3). The strong ^{13}C DEP, SEP and FEP lines from

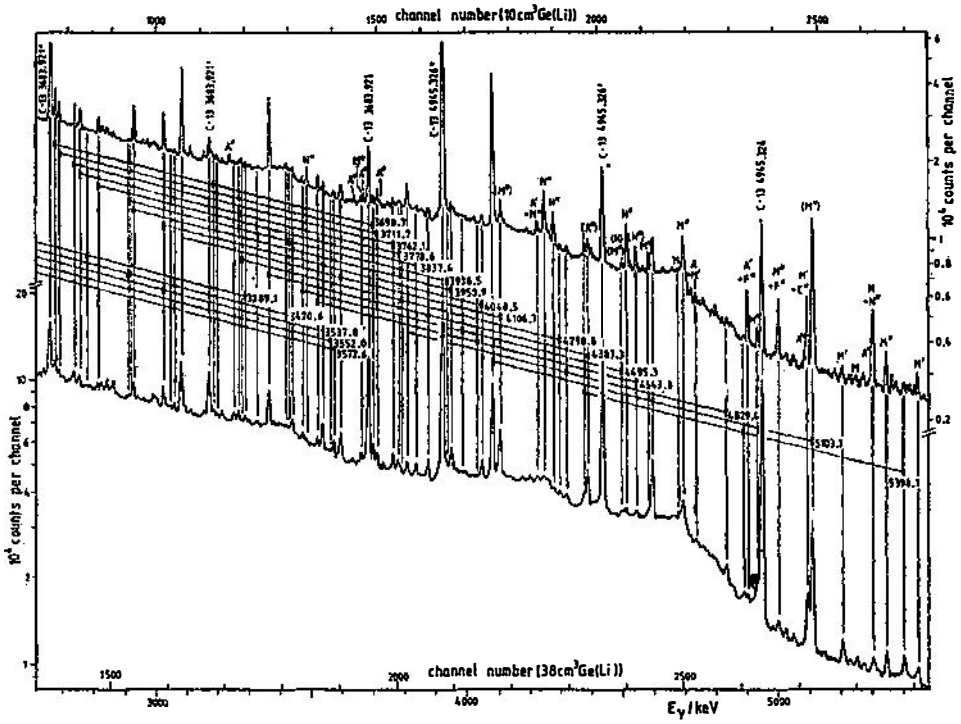

Fig. 3. Parts of high-energy γ-ray spectra measured with two Ge (Li) detectors of different ratios of double-escape peaks (labelled by double primes) and single-escape peaks (labelled by primes) to full-energy peaks. The background lines are labelled with A for ^{27}Al (n, γ); N for ^{14}N (n, γ), C for ^{35}Cl (n, γ), F for ^{56}Fe (n, γ) and M for ^{95}Mo (n, γ). Brackets around these labels indicate admixture to a line from ^{101}Mo. The positions of double escape, single escape, and full energy peaks from ^{100}Mo (n, γ) are indicated by connecting lines between the spectra.

neutron capture in the graphite target capsule (E_γ = 1261.788 keV[26], 3683.921 keV[27] and 4945.326 keV[28,29]) were used for energy calibration and correction for nonlinearity under the assumption that the DEP, SEP and FEP energy differences are[30] m_0c^2. The relative DEP, SEP and FEP efficiencies and efficiency ratios were determined with these lines[31] and those from the ^{14}N (n, γ) reaction[32].

Using the energy overlap of the various recorded spectra, absolute γ-ray intensities for the secondary as well as for the high-energy primary transitions have been derived by normalization to the intensity of the strong ^{101}Tc transition of 191.9 keV for which I_γ = 18.8 (4)/100 decays[7].

With use of 38 and 63 cm^3 Ge (Li) detectors, γ-γ coincidences have been measured for $40 \leq E_{\gamma 1}, E_{\gamma 2} \leq 5800$ keV. Two characteristic coincidence spectra are shown in Fig. 4. The data resulting from the singles and coincidence measurements are given in Section 3 together with those from the β^--decay study.

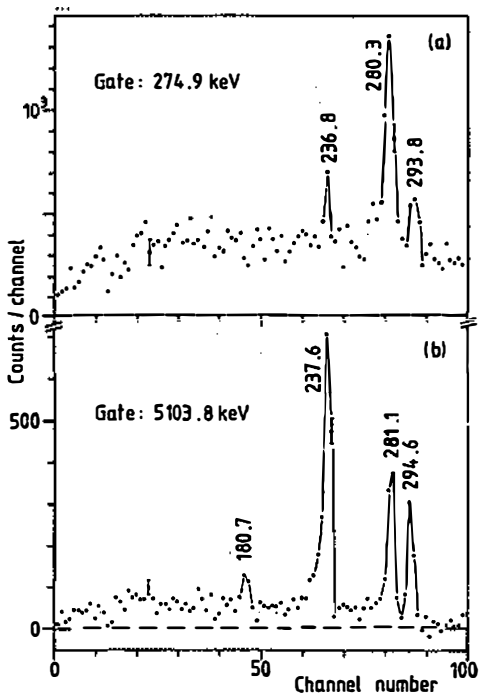

Fig. 4. Gamma-ray spectra observed in coincidence with the 274.9 keV transition feeding the 293.8 keV state (a) and the 5103.8 keV primary transition feeding the near-lying 294.6 keV state (b). Both spectra result after subtraction of adjacent Compton-background spectra.

2.3. *Angular distributions and relative cross-sections from the $^{100}Mo\,(d,p)$ reaction*

The reaction ^{100}Mo (d, p) was investigated with high resolution (5 keV) at the Munich MP tandem using the Q3D spectrograph in conjunction with the precision time-of-flight system in order to correct energy fluctuations of the 14 MeV deuteron beam. ^{100}Mo metal targets were prepared by electron-beam evaporation. On 4—5 μg/cm^2 carbon backings, line targets (0.5 mm · 4 mm) enriched to 97.4% in ^{100}Mo of 40—60 μg/cm^2 were deposited. Proton spectra were measured at 8 laboratory angles (6°, 14°, 20°, 30°, 35°, 45°, 50° and 60°) and detected with a multiwire proportional counter with 800 wires spaced at 0.5 mm. A typical proton spectrum is shown in Fig. 5. In the analysis of the data 19 levels could be identified in the excitation energy range of 0—583 keV. Their angular distributions and relative differential cross sections are shown in Figs. 6a and 6b. Further details about the experimental technique and the analysis of the data can be taken from Ref. 33. These measurements were carried out in the last beam time before the

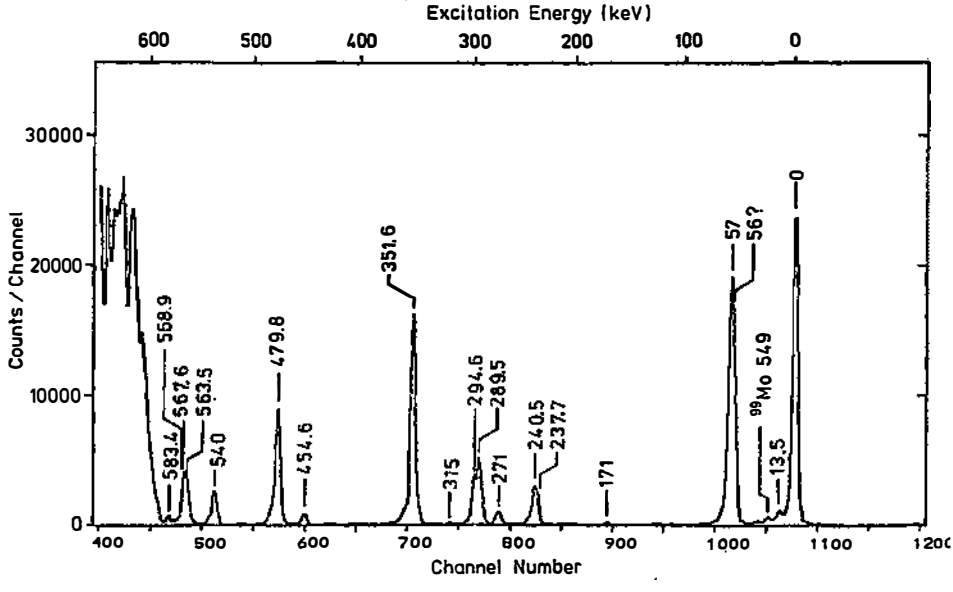

Fig. 5. Proton spectrum observed in the ^{100}Mo (d, p) reaction at $\Theta_{lab} = 14°$.

first upgrading of the München MP tandem in 1975, they remained unpublished until now.

For those levels which are also observed in the (n, γ) study, the more accurate energy values from this work were adopted and used for more precise calibration of the other levels. For the analysis of overlapping lines different situations had to be solved: In the case of the 57 keV peak a slight broadening, especially at laboratory angles above 30°, indicates a possible doublet of states as is discussed in Ref. 14. The peak at about 565 keV in a first analysis seemed to contain two components. However, the higher-energetic of them showed no interpretable angular distribution. According to the (n ,γ) results it was tried to fit a third component into this peak. The unambiguous angular distributions which then were obtained support the existence of a triplet of near-lying states which are discussed below.

3. *Discussion of experimental results and particular levels*

The γ-ray energies of transitions in ^{101}Mo, their absolute intensities per 10^3 radiative slow neutron captures in ^{100}Mo and their relative intensities in β^- decay of ^{101}Nb are collected in Table 2. The observed coincidence relationships are presented in Table 3. The ^{101}Mo level scheme which results from the present studies is depicted in Figs. 7 and 8. The properties of all ^{101}Mo states as known from other experimental studies and the present work are collected in Table 4. The γ-decay patterns of Figs. 7 and 8 result from the (n, γ) study or (for the states marked by an asterik) from the (n, γ) study and the investigations at LOHEN-

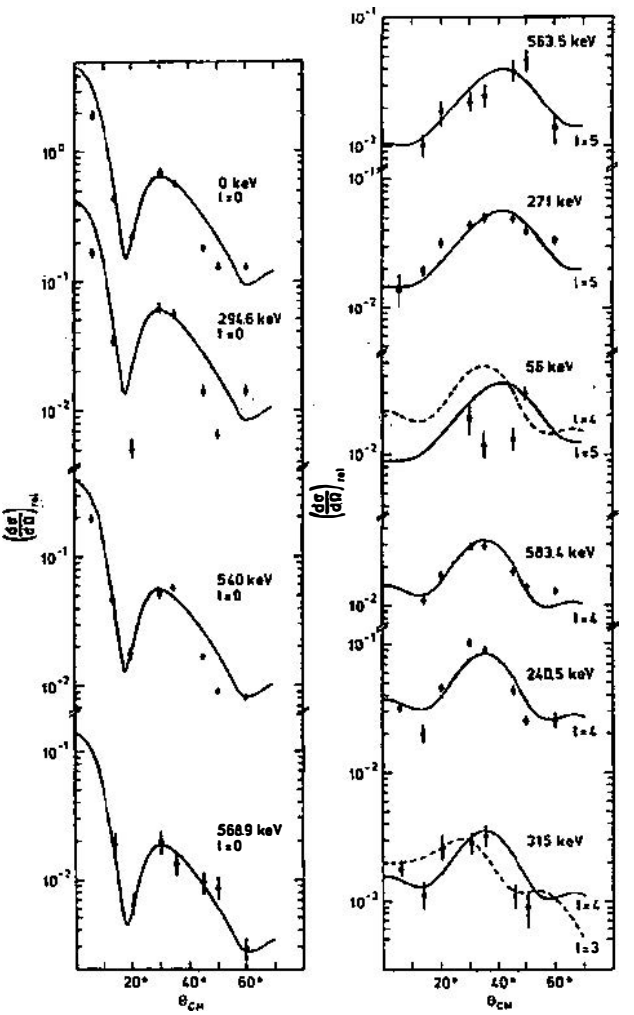

Fig. 6a. Observed proton angular distributions with $l_n = 0, 3, 4, \text{or} 5$.

GRIN. To deduce the averages from the two sets of data (Table 2), for each measurement the γ-ray intensity of the stronges transition depopulating a state has been normalized to 100. With this normalization the relative γ-ray intensities of the weaker transitions have been deduced as weighted averages from the results of both measurements taking into account the error of the intensity of the strongest transition by quadratic addition of the errors.

The population of the low-lying states by the statistical cascades from the capture state via the quasi-continuum of higher-lying states has been calculated using a computer code[37] described in Ref. 38. In Fig. 9 the calculated values are compared with the experimental data. An overall agreement within 30% is obtained.

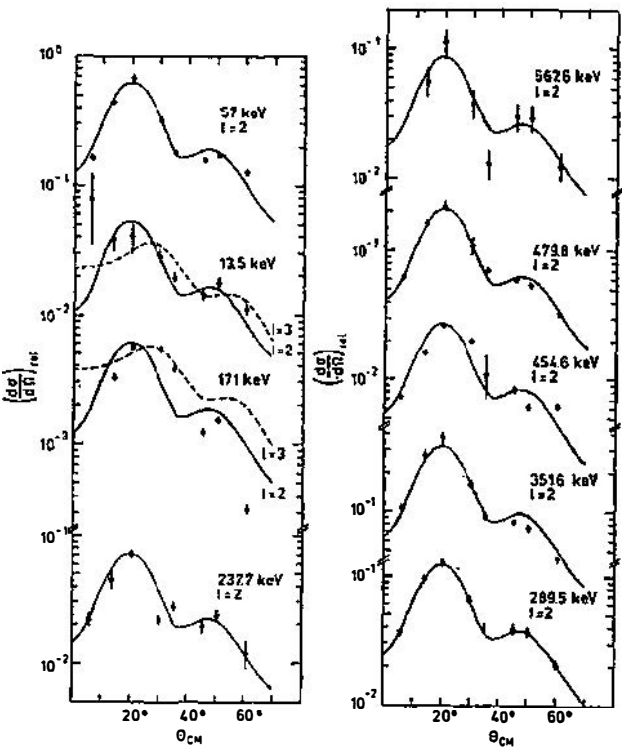

Fig. 6b. Observed proton angular distributions with $l_n = 2$ or 3.

The statistical population of a low-lying state depends strongly on its spin difference to the $J = 1/2$ capture state. The calculated values of Fig. 10 set lower limit for the total depopulation of the low-spin states ($J \leq 5/2$). The sum of the statistical population and the population from the established discrete states ($E_{ex} \leq \leq 1447$ keV) and the capture state yields the total population of a state which must be equal to the total depopulation within the error.

The level schemes of Figs. 7 and 8 do not contain the levels at 329.3, 666.3, 716.9 and 839.2 keV which were given in a preliminary report on the (n, γ) study[7,10] only because of the possible occurence of weak primary transitions of 5069.3, 4732.3, 4681.7 and 4559.4 keV, respectively. The assumption of E1, M1 or E2 character for these transitions allows $J^\pi = 1/2^+$, $3/2^+$ or $5/2^+$ for the four levels. However, no secondary transitions are found in the low-energy spectra which could satisfy the lower limits of Fig. 9 for the depopulation of these states. In agreement with this, the reanalysis of the spectra of Fig. 3 has shown that the FEP and SEP intensities (explanation see Section 2.2) of the strong 4048.6 and 3537.8 keV transitions leave no line intensity for the DEP of a 5069.3 keV transition and the SEP and DEP of a 4559.4 keV transition. The 4732.2 and 4681.7 keV DEP, SEP and FEP can be assigned to transitions from ^{27}Al (n, γ)[23] and ^{95}Mo (n, γ)[39].

TABLE 2.

(n,γ)		β^- decay			
E_γ (dE_γ)[a] /keV	I_γ (dI_γ)[a] /10^3 n	E_γ (dE_γ)[a] /keV	I_γ (dI_γ)[a] rel. units	position[b]	
13.49(10)	78 (29)	13.5(1)	32 (10)	13.5	0.0[c]
37.0(4)	0.6(2)			(351.6	315)
43.515(5)	23.7(16)	43.5(1)	4 (1)	57.0	13.5[c]
56.892(20)	1.32(18)			294.6	237.7
81.122(5)	39.7(17)	81.2(1)	1.0(2)	318.9	237.7[c]
113.935(10)	5.3(3)	114.0(1)	2.0(2)	171.0	57.0[c]
118.556(11)	5.3(3)	118.6(1)	14(1)	289.5	171.0[c]
123.0(3)	0.4(2)			293.8	171.0
				294.6	171.0
124.2(2)	0.5(3)			1099.4	974.8
125.057(11)	5.2(3)			1109.2	984.2
138.4(2)	2.2(7)				
140.8(2)	2.4(6)			710.0	568.9[c]
143.1(1)	1.2(4)			(315	171.0)
147.935(18)	4.1(10)			318.9	171.0[c]
157.466(12)	81.2(10)	157.5(1)	32 (2)	171.0	13.5[c]
164.0(2)	0.9(4)			974.8	810.6
				1281.2	1116.9
164.96(15)	0.9(4)	165.0(3)[d]	0.2(1)[d]	454.5	289.5[c]
165.90(25)	0.7(5)			1447.3	1281.2
180.703(19)	109 (2)	180.6(1)	8.8(6)	237.7	57.0[c]
180.8(3)[d]	2.0(5)[d]			351.6	171.0[c]
181.5(2)	3.2(5)			1291.3	1109.2[c]
182.1(5)	1.1(5)			(240.5	57.0)
185.96(5)	2.8(6)	186.0(3)	2.6(2)	479.8	293.8[c]
188.46(6)	1.2(5)			540.1	351.6
189.8(2)	1.0(5)			479.8	289.5
202.5(2)	0.8(5)			1116.9	914.2
204.06(6)	1.4(5)			830.4	626.4
216.82(3)	2.4(5)	217.0(2)	1.2(2)	454.5	237.7[c]
218.2(4)	1.6(7)			1229.8	1011.0
				1447.3	1229.8
223.8(3)	3.7(8)	224.0(2)	0.7(2)	237.7	13.5[c]
230.18(7)	2.7(5)			710.0	479.8[c]
231.1(2)	1.2(6)			1054.3	823.1
				1099.0	867.8
232.4(2)	2.0(8)	232.6(1)	4.9(4)	289.5	57.0[c]
233.3(2)	2.9(8)				
234.1(2)	3.4(8)			1281.2	1047.1[(c)]
236.78(4)	12.6(11)	236.8(3)[d]	1.5(5)[d]	293.8	57.0[c]
237.55(2)	95.0(20)			294.6	57.0[c]
238.4(5)	1.3(7)	237.5(5)[d]	0.2(2)[d]	237.7	0.0[(c)]
241.38(5)	1.0(2)			867.8	626.4
				1109.2	867.8
274.9(2)	6.6(18)			568.9	293.8[c]
276.10(4)	56.8(12)	276.1(1)	≡100 (6)	289.5	13.5[c]
277.98(4)	4.8(9)			567.5	289.5[c]
280.25(4)	36.8(9)	280.3(1)	3.4(4)	293.8	13.5[c]
281.05(4)	45.5(12)			294.6	13.5[c]
283.5(2)	4.2(19)	283.5(1)	3.3(4)	454.5	171.0[c]
287.86(11)	3.0(14)			914.2	626.4
289.63(5)	6.7(13)	289.6(1)	10.0(8)	289.5	0.0[c]
292.0(2)	4.0(22)			586.5	294.6

TABLE 2 continued.

(n,γ)		β^- decay			
E_γ (dE_γ)[a] /keV	I_γ (dI_γ)[a] /10^3 n	E_γ (dE_γ)[a] /keV	I_γ (dI_γ)[a] rel. units	position[b]	
293.81(11)	20.3(5)	294.0(5)[d]	2 (1)[d]	293.8	0.0[e]
294.59(4)	43.7(29)[d]			294.6	0.0[e]
294.59(4)	37.7(32)[d]	294.5(3)[d]	5 (2)[d]	351.6	57.0[e]
305.5(2)	74 (7)	305.2(2)	0.9(3)	318.9	13.5[e]
309.0(3)	7.4(12)				
311.21(17)	2.3(13)				
317.5(3)	2.1(13)			797.2	479.8[e]
326.45(10)	0.9(3)			909.8	583.4
329.93(6)	4.1(3)			567.5	237.7[(c)]
331.2(3)	1.8(3)			568.9	237.7[(c)]
335.34(5)	2.2(3)			902.8	567.5
338.5(3)	1.4(3)	338.1(2)	0.2(2)	351.6	13.5
340.5(2)	1.2(3)			909.8	568.9
343.4(2)	1.4(3)			823.1	479.8
351.595(15)	19.9(14)	351.6(1)	2.4(3)	351.6	0.0[e]
355.7(3)	0.5(3)	356.3(2)	0.8(3)	810.6	454.5[e]
358.41(4)	4.3(5)			710.0	351.6[e]
364.99(15)	2.2(13)				
367.5(2)	2.1(12)			1281.2	914.2
369.79(5)	4.(2)			909.8	540.1[e]
374.6(2)	0.6(4)	374.5(5)	0.4(2)	854.1	479.8[e]
388.59(7)	4.6(14)			626.4	237.7[e]
392.9(4)	2.5(14)			1447.3	1054.3
395.8(3)	3.8(4)				
398.0(3)	1.6(9)[d]	397.5(5)	1.4(3)	454.5	57.0
398.0(3)	4.3(26)[d]			568.9	171.0[e]
399.0(2)	5 (2)	399.3(5)	2.8(6)	854.1	454.5[e]
406.80(6)	3.5(14)			1116.9	710.0
				1229.8	823.1
412.1(3)	3.9(18)			583.4	171.0[e]
414.6(3)	1.0(5)				
415.9(3)	2.8(13)			710.0	293.8[e]
420.43(3)	5.4(8)			710.0	289.5[e]
423.3(4)	0.8(5)	422.8(2)	0.5(3)	479.8	57.0
436.7(5)	2.7(15)			1291.3	854.1
441.01(5)	19.4(19)	441.1(1)	22(1)	454.5	13.5[e]
454.0(3)	3.3(16)	454.5(2)	1.7(5)	454.5	0.0[e]
459.0(3)	3.3(18)	459.1(2)	1.9(4)	810.6	351.6[e]
466.35(4)	18.4(15)	466.3(1)	18(1)	479.8	13.5[e]
480.1(4)	12 (4)	479.8(1)	19(1)	479.8	0.0[e]
507.2(7)	1.5(4)	507.5(3)	4.0(6)	797.2	289.5[e]
526.55(5)	18.5(13)			540.1	13.5[e]
539.6(3)	6.0(15)			710.0	171.0[e]
540.21(17)	10.7(20)			540.1	0.0[e]
554.2(5)	2.6(17)			567.5	13.5
555.34(6)	17.5(12)			568.9	13.5[e]
559.4(2)	1.3(5)	559.7(2)	3.3(5)	797.2	237.7[e]
560.3(5)	3.8(16)			854.1	293.8[e]
567.4(3)	9.5(10)			567.5	0.0
569.17(7)	6.7(6)			1109.2	540.1[e]
583.96(3)	15.8(20)			902.8	318.9[e]
586.40(14)	11 (1)			586.5	0.0
603.69(15)	2.6(5)			1229.8	626.4
608.21(2)	14.1(25)			902.8	294.6[e]
616.78(14)	1.7(3)			1447.3	830.4

TABLE 2 continued.

(n, γ)		β^- decay			
E_γ (dE_γ)[a] /keV	I_γ (dI_γ)[a] /10^3 n	E_γ (dE_γ)[a] /keV	I_γ (dI_γ)[a] rel. units	position[b]	
620.8(3)	1.2(3)			909.8	289.5
				914.2	293.8
623.38(17)	4.7(3)			974.8	351.6[c]
626.17(10)	2.2(8)	626.1(2)	0.9(3)	797.2	171.0[c]
630.1(4)	1.1(6)			867.8	237.7[c]
631.79(10)	2.6(3)			1199.4	567.5
634.6(2)	1.5(8)				
636.7(2)	1.6(3)			1447.3	810.6
639.62(7)	3.8(14)	639.5(3)	0.8(3)	810.6	171.0[c]
645.7(2)	3.9(3)				
651.1(3)	2.9(6)				
652.5(2)	0.9(2)			823.1	171.0
657.9(4)	0.9(3)				
664.9(2)	3.4(14)			902.8	237.7
679.4(3)	2.7(3)				
682.9(2)	4.7(4)	682.9(2)	3.2(6)	854.1	171.0[c]
691.7(3)	4.3(3)			1011.0	318.9
695.0(5)	11 (5)			1047.1	351.6[c]
696.2(2)	10 (2)			867.8	171.0[c]
697.7(2)	3 (2)			1281.2	583.4[c]
707.5(3)	2.8(3)				
716.41(7)	36 (2)			1011.0	294.6[c]
719.67(7)	13.2(14)			1199.4	479.8[c]
722.44(6)	10.6(27)			1291.3	568.9[c]
737.0(1)	4.5(6)			974.8	237.7[c]
740.3(2)	1.4(10)	740.2(2)	1.7(4)	797.2	57.0
753.8(2)	1.3(9)	753.6(4)	0.8(3)	810.6	57.0
757.8(3)	2.9(8)			1109.2	351.6[c]
760.1(3)	2.2(9)			1054.3	294.6[c]
765.9(2)	7 (2)			1116.9	351.6[c]
783.6(3)	3.8(9)	783.5(2)	7.4(15)	797.2	13.5
790.0(5)	2.7(8)			1109.2	318.9
797.10(21)	6.0(5)	797.1(2)	7.2(12)	854.1	57.0
806.7(2)	3.1(6)				
810.8(4)	5.3(3)	810.6(4)	2.5(12)	810.6	0.0
814.9(2)	1.7(4)			1109.2	294.6
823.08(6)	6.0(15)			823.1	0.0
840.63(15)	3.4(7)	840.5(3)	1.4(3)	854.1	13.5
853.1(3)	5.7(4)			909.8	57.0
854.1(2)	5.3(7)	853.9(2)	4.6(9)	854.1	0.0
902.98(10)	5.3(4)			902.8	0.0
918.5(5)	5 (2)			974.8	57.0
924.51(15)	3.3(3)				
926.3(5)	4 (2)			984.2	57.0
929.1(2)	4.6(4)				
940.4(5)	6.7(7)			1229.8	289.5[c]
962.4(2)	4.4(4)			1281.2	318.9
967.9(3)	13.4(15)			1447.3	479.8[c]
970.9(2)	11.2(25)			984.2	13.5
972.6(3)	32 (2)			1291.3	318.9[c]
973.4(3)	9.6(18)				
997.58(10)	1.8(4)			1011.0	13.5[c]
1007.8(2)	4.7(5)				
1025.02(10)	3.8(4)				
1030.85(10)	9.3(5)			1349.7	318.9[c]

TABLE 2 continued.

(n, γ)		β^- decay			
E_γ (dE_γ)[a] /keV	I_γ (dI_γ)[a] /10^3 n	E_γ (dE_γ)[a] /keV	I_γ (dI_γ)[a] rel. units	position[b]	
1042.6(5)	12.0(20)	1042.2(2)	3.6(7)	1099.0	57.0
1052.8(3)	8.0(6)			1109.2	57.0
1054.4(3)	7.0(5)			1054.3	0.0
1074.8(2)	0.5(2)				
1084.8(6)	2.6(10)	1085.7(3)	1.2(6)	1099.4	13.5
1097.48(10)	8.4(4)				
1107.9(2)	4.2(5)				
1119.9(3)	12 (2)			1291.3	171.0[c]
1127.8(2)	1.5(5)			1447.3	318.9
1130.6(2)	1.6(6)				
1153.0(3)	7.0(8)			1447.3	294.6[c]
1157.5(3)	7.8(8)			1447.3	289.5[c]
1208.1(2)	2.1(5)				
1229.70(10)	3.1(4)			1229.8	0.0
1235.63(15)	1.0(4)				
1278.5(2)	0.5(2)				
1287.3(3)	3.9(5)				
1300.32(15)	6.1(6)				
1315.2(3)	1.8(4)				
1405.57(15)	5.7(4)				
1433.2(2)	13.5(11)				
1440.4(2)	2.0(5)				
1447.7(4)	3.9(6)			1447.3	0.0
3289.1(8)[e]	7.8(13)				
3420.6(10)[e]	3.5(9)				
3537.8(2)[e]	15.8(11)				
3552.0(6)[e]	3.7(5)				
3572.6(3)[e]	12.8(9)				
3698.7(2)[e]	19.1(13)				
3711.7(4)[e]	11.7(8)				
3762.1(3)[e]	12.3(6)				
3778.6(3)[e]	9.1(7)				
3837.4(4)[e]	7.7(6)				
3938.5(4)[e]	6.9(13)				
3950.9(2)	16.8(13)			5398.3	1447.3[c]
4048.5(2)	14.7(8)			5398.3	1349.7[c]
4106.7(2)	41.7(15)			5398.3	1291.3[c]
4298.8(4)	3.7(4)			5398.3	1099.0
4387.3(2)	26.5(13)			5398.3	1011.0[c]
4495.3(3)	3.5(7)			5398.3	902.8
4543.8(3)	4.6(3)			5398.3	854.1[c]
4829.4(2)	6.2(4)			5398.3	568.9[c]
5103.7(2)	68 (3)			5398.3	294.6[c]
5398.1(3)	5.0(4)			5398.3	0.0

[a] The numbers within brackets give the errors of the last given digits. The first column gives the γ-ray energies without recoil correction. The absolute γ-intensity errors do not contain the 2% error of the 191.9 keV transition intensity in ^{101}Tc which was used for absolute calibration.

[b] The numbers give the energies of the initial and final state in keV. Brackets indicate tentative positions of weak transitions connected with the states of $J \geq 7/2$.

[c] This label indicates confirmation by at least one observed coincidence relationship, (c) denotes a questionable coincidence.

[d] Deduced from the coincidence data.

[e] Primary transitions to states between 1459.7 and 2109.2 keV which are not discussed in the present work.

Gamma-ray transitions observed in the present ^{100}Mo (n, γ) and ^{101}Nb β^--decay studies.

TABLE 3.

Lower-lying transition/keV	Coincident transitions[a]/keV
13.5	43.5, 118.6, 157.5, 180.7, 232.6, 276.1, 280.3, 294.6, 441.0, 466.3
43.5	113.9, 180.7, 232.6, 294.6
81.1	584.0, 972.6, 1030.9, 4048.6, 4106.8
113.9	118.6′
118.6	420.4
147.9	584.0, 972.6, 4106.8
157.5	118.6″, 147.9, 180.8, 283.5″, 398.0, 412.1, 539.6, 626.2″, 639.6″, 682.9″, 696.2, 972.6, 1119.9, 4106.8, 4543.9
180.7	81.1″, 216.8″, 329.9(+331.2), 388.6, 559.6′, 584.0, 630.1, 716.4, 737.0, 972.6, 1030.9, 4048.6, 4106.8, 5103.8
181.5	4106.8
223.9	81.1′
236.8	186.0″, 274.9, 415.9, 560.3
237.6	608.2, 716.4, 760.1, 1153.0, 3951,0. 4387.3, 5103.8
238.0	(81.1′)
276.1	165.0″, 278.0, 420.4, 507.5″, 940.4, 1157.5
280.3	186.0″, 274.9, 415.9, 560.3
281.1	608.2, 716.4, 1153.0, 4387.4, 5103.8
289.6	278.0
293.8	186.0″, 274.9, 415.9, 560.3
294.6	358.4, 459.1, 608.2, 623.4, 695.0, 716.4, (757.8), 1153.0, 4387.4, 5103.8
305.4	584.0, 972.6, 1030.9, 4048.6, 4106.8
351.6	358.4, 459.1, 623.4, 695.0, 757.8, 765.9
412.1	697.7
441.0	356.1″, 399.0
454.3	399.0′
466.3	230.2, 374.6′, 719.7, 967.9
479.8	230.2, 317.5, 374.6′, 719.7, 967.9
526.6	369.8, 569.2
540.2	369.8, 569.2
555.3	140.8, 722.4, 4829.5
695.0	(234.1)
716.4	4387.4
722.4	4106.8
967.9	3951.0
972.6	4106.8
997.6	4387.4
1030.9	4048.6
1052.8	181.5
1153.0	3951.0

[a] Coincidences with the low-energy transitions of 13.5 and 43.5 keV only have been investigated in the ^{101}Nb β^- decay studies. Most of the coincidence relations between transitions of higher energy result from the ^{100}Mo(n, $\gamma - \gamma$) study. Those which could be observed only at LOHENGRIN are marked by a single prime, whereas double primes denote coincidence relations measured after neutron capture and at LOHENGRIN.

Observed coincidence relations for transitions in ^{101}Mo.

TABLE 4.

E_{ex}[a]/keV	l_n	(d, p) from Ref.	$(2J+1)\,S$[b]	$J\pi$ $(\vec{d},p)$, $(\vec{t},d)$[b,c]	$J\pi$ $(n_{res}\,\gamma)$[d]	$J\pi$ present work	$J\pi$ resulting assignment
0	0	b, c, e, f, g	0.366(6)	$1/2^+$		$1/2^+$	$1/2^+$
13.497(9)	2,3	g	<0.02[h]		$(3/2)^+$	$3/2^+$	$3/2^+$
56(1)[i]	4,5[i]	g				$>7/2^+$[i]	$>7/2^+$[i]
57.015(11)	2	b, c, e, f, g	0.390 (36)	$5/2^+$	$3/2^+$[j]	$3/2^+$, $5/2^+$	$5/2^+$
170.958(14)	2,3	c, g			$(5/2^+)$	$3/2^+$, $5/2$	$(5/2^+)$
237.732(15)	2	g		$7/2^+$		$3/2^+$, $5/2^+$[k]	$3/2^+$, $5/2^+$[k]
240.5(10)	4	g				$7/2^+$, $9/2^+$	$7/2^+$, $9/2^+$
271(1)	5	b, c, g, l	1.18 (14)	$(11/2)^-$		$9/2^-$, $11/2^-$	$9/2-$, $11/2-$
289.531(17)	2	g		$3/2^+$	$3/2^+$	$3/2^+$, $5/2^+$	$3/2^+$
293.786(26)						$1/2^+$, $3/2$, $5/2^+$	$1/2^+$, $3/2$, $5/2^+$
294.586(16)	0	g				$1/2^+$	$1/2^+$
315 (3)	3,4	g				$7/2$, $9/2^+$	$7/2$, $9/2^+$
318.858(18)					$(5/2)^+$	$1/2^+$, $3/2^+$, $5/2^+$[k]	$(5/2)^+$[k]
351.589(19)	2	b, c, g	0.43 (4)	$3/2^+$	$(5/2)^+$	$3/2^+$, $5/2^+$	$3/2^+$
454.549(39)	2	g		$(5/2)^+$	$3/2^+$[m]	$3/2^+$, $5/2^+$	$(5/2)^+$
479.777(36)	2	b, c, g	0.204 (12)	$3/2^+$	$(3/2)^+$	$3/2^+$, $5/2^+$	$3/2^+$
540.053(35)	0	b, c, g	0.036 (10)	$1/2^+$		$1/2+$	$1/2^+$
563.5(10)	5	g				$9/2^-$, $11/2^-$	$9/2^-$, $11/2^-$
567.546(30)	2	g	0.114(6)	$5/2^+$		$5/2^+$	$5/2^+$
568.85(6)	0	g				$1/2^+$	$1/2^+$
583.39(12)	4	b, c, g				$7/2^+$, $9/2^+$	$7/2^+$, $9/2^+$
586.47(12)						$1/2$, $3/2$	$1/2$, $3/2$
626.36(5)						$7/2$, $9/2$	$7/2$, $9/2$
709.981(27)	(0)	e	0.04		1/2, 3/2	$1/2^{(+)}$, $3/2$	$1/2^{(+)}$ $(3/2)$
797.16(8)	(1)	e	0.07		1/2, 3/2	$1/2^+$, $3/2$	$1/2^+$, $3/2$
810.60(6)						$1/2^{(+)}$, $3/2$, $5/2^+$	$1/2^{(+)}$, $3/2$, $5/2^+$
823.09(5)					$\pi = (+)$	$1/2^{(+)}$, $3/2$, $5/2^{(+)}$	$1/2^{(+)}$, $3/2^{(+)}$, $5/2^{(+)}$
830.43(7)	4	b, c	0.248(32)			$7/2^+$ $(9/2)^+$	$7/2^+$ $(9/2)^+$
854.07(8)					$\pi = (+)$	$1/2+$, $3/2$	$1/2^+$, $3/2^{(+)}$
867.78(8)	2	b, c	0.056(8)	$3/2^+$			$3/2^+$
902.842(28)	0,2(1)	f	0.03, 0.05			$1/2^{(+)}$, $3/2$	$1/2^{(+)}$, $3/2$
909.83(8)						$3/2^+$, $5/2^+$ (1/2)	$3/2^+$, $5/2^+(1/2)$
914.19(13)	4	b, c	0.160(24)	$(7/2)^\pm$		$7/2$, $9/2^+$	$(7/2)^+$
974.78(8)						$1/2^{(+)}$, $3/2$, $5/2^{(+)}$	$1/2^{(+)}$, $3/2$, $5/2^{(+)}$

TABLE 4 continued.

E_{ex}[a]/keV	l_n	(d, p) from Ref.	$(2J+1)\,S$[b]	$J\pi$ $(\vec{d},p)$, $(\vec{t},d)$[b,c]	$J\pi$ (n_{res},γ)[d]	$J\pi$ present work	$J\pi$ resulting assignment
984.17(7)	2	b, c	<0.036	$3/2^+, 5/2^+$			$3/2^+, 5/2^+$
1011.01(6)	(0)	e	0.08			1/2, 3/2	$1/2^{(+)}$, (3/2)
1047.05(21)	0	b, c	0.010(4)				$1/2^+$
1054.34(14)						$1/2, 3/2, 5/2^+$	$1/2, 3/2, 5/2^+$
1098.99(13)						$1/2^{(+)}$, 3/2	$1/2^{(+)}$, 3/2
1109.23(7)	2	b, c	0.064(4)	$3/2^+$			$3/2^+$
1116.86(12)						$3/2^{(+)}$, 5/2(1/2)	$3/2^{(+)}$, 5/2 (1/2)
1199.41(6)						$1/2^{(+)}$, 3/2, 5/2	$1/2^{(+)}$, 3/2, 5/2
1229.84(8)						3/2, 5/2	3/2, 5/2
1281.22(11)						$3/2^+, 5/2^{(+)}$	$3/2^+, 5/2^{(+)}$
1291.25(9)	1	b, c	0.116(12)	$3/2^-$		$3/2^-$	$3/2^-$
1349.71(9)						1/2, 3/2	1/2, 3/2
1447.28(9)						$3/2^{(+)}$ (1/2)	$3/2^{(+)}$ (1/2)

[a] Present work. The numbers within brackets give the error of the last given digits.

[b] From Ref. 7.

[c] From Ref. 9.

[d] From Ref. 8.

[e] From Ref. 34.

[f] From Ref 35.

[g] Present (d, p)-reaction study.

[h] Deduced from the observed proton intensity (Fig. 5) relative to the 57 keV peak under the assumption $l_n = 2$.

[i] Questionable state, see Section 3 and Ref. 14.

[j] See comments Section 3 and Ref. 14.

[k] $M1 + E2$ character of the 81.1 keV transition postulates same parity and spin difference ≤ 1 for the 237.7 keV $3/2^+$ or $5/2^+$ state and the 318.9 keV state.

[l] From Ref. 36.

[m] See comments Section 3.

Properties of the ^{101}Mo states for $E_{ex} \leq 1447.2$ keV as deduced from the present and other experiments.

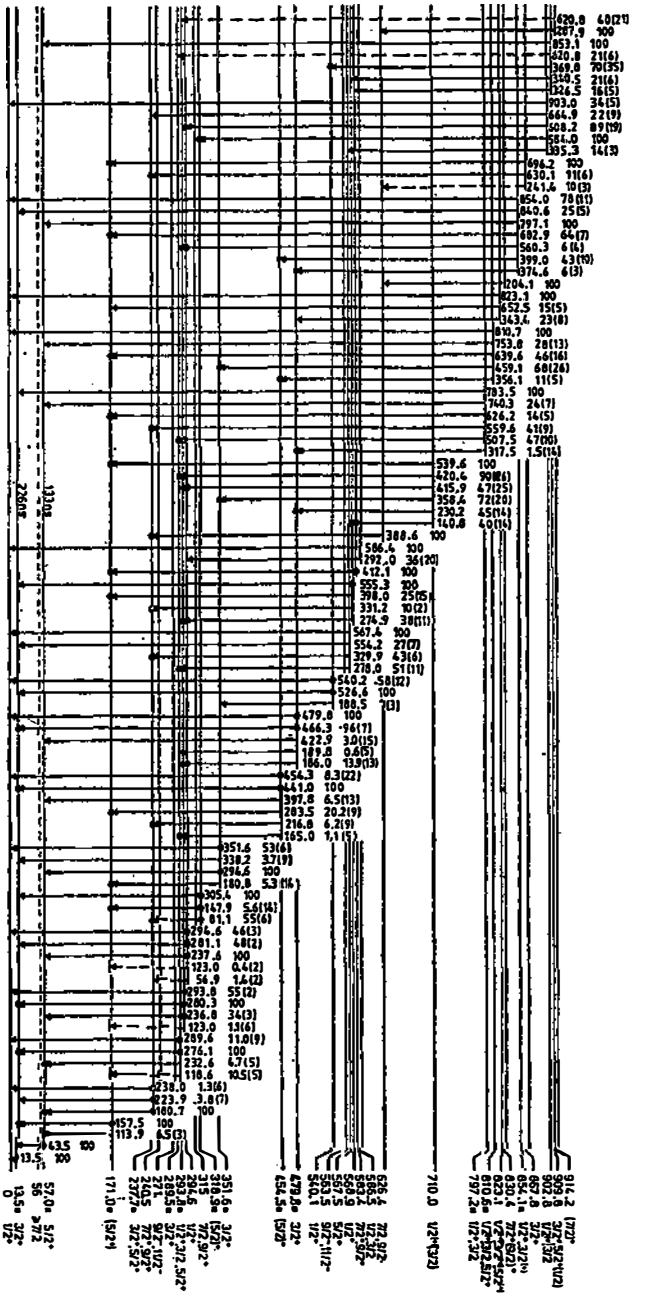

Fig. 7. The ^{101}Mo level scheme resulting from the present experiments for $E_{ex} \leq 914.2$ keV. Full points at the lower (upper) end of a transition indicate that at least one coincidence with a lower (higher)-lying transition was observed. Open circles indicate questionable coincidences. Transitions which can be placed twice are given as dashed lines. The transitions are labelled by their energy and the relative γ-ray intensity (see text, Section 3). Those states which were established also in the β^-decay study are marked by an asterisk.

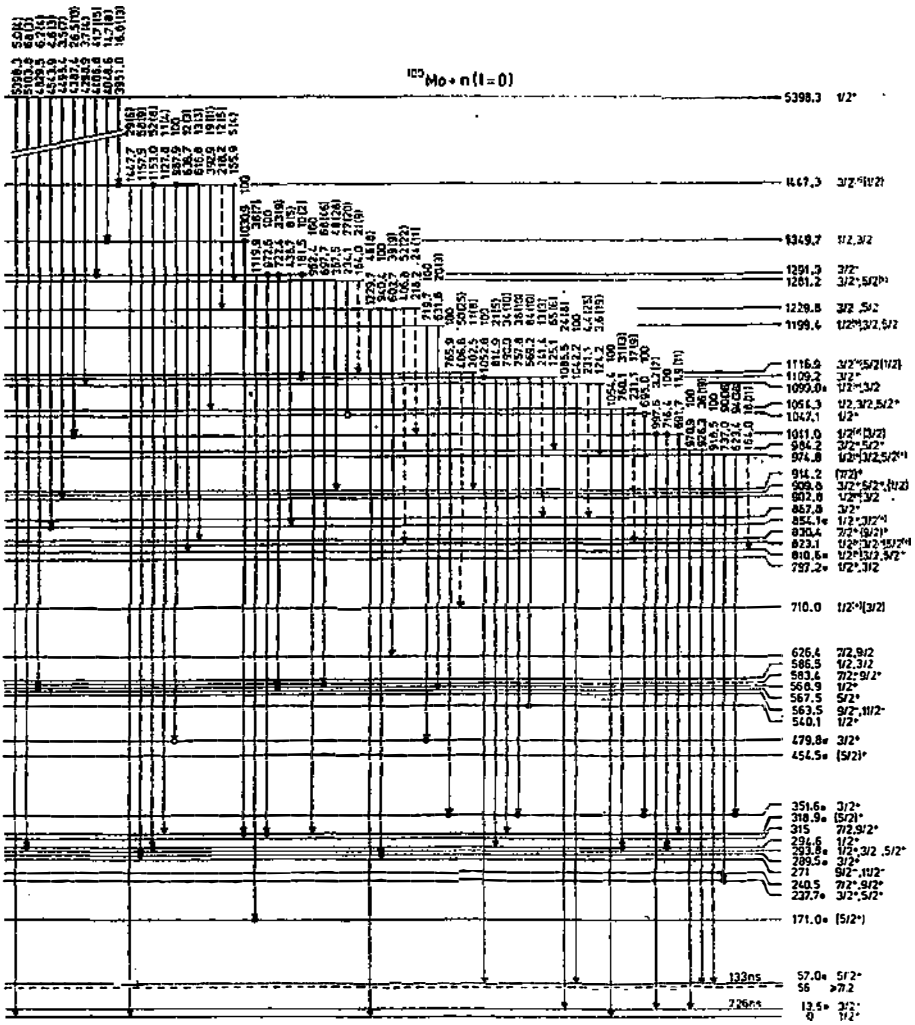

Fig. 8. The present ^{101}Mo level scheme for $E_{ex} \leq 1447.3$ keV and the slow neutron capture state with the transitions from states with $E_{ex} > 914.2$ keV (further explanations see Fig. 8). For the primary transitions from the capture state the γ-transition intensities are given per 10^3 radiative neutron captures.

The present level scheme for $E_{ex} \leq 1447.3$ keV and the primary transitions of Fig. 8 yield the neutron binding energy as $S_n = 5398.27(8)$ keV in agreement with the less accurate preliminary value of 5398.4(5) keV[10,19]. According to the used ^{12}C (n, γ) calibration energies the given value of S_n finally is based upon the remeasurement of the ^{198}Au 411.8 keV line[40]. The energies of the low-lying states are based upon the energies of the secondary γ-rays. Their systematic error can be estimated from the fitted Mo and Pb K X-ray energies which are given in Fig. 2. These energies (with total fitting errors) of 17.436(5) keV for Mo K$\alpha_{1,2}$,

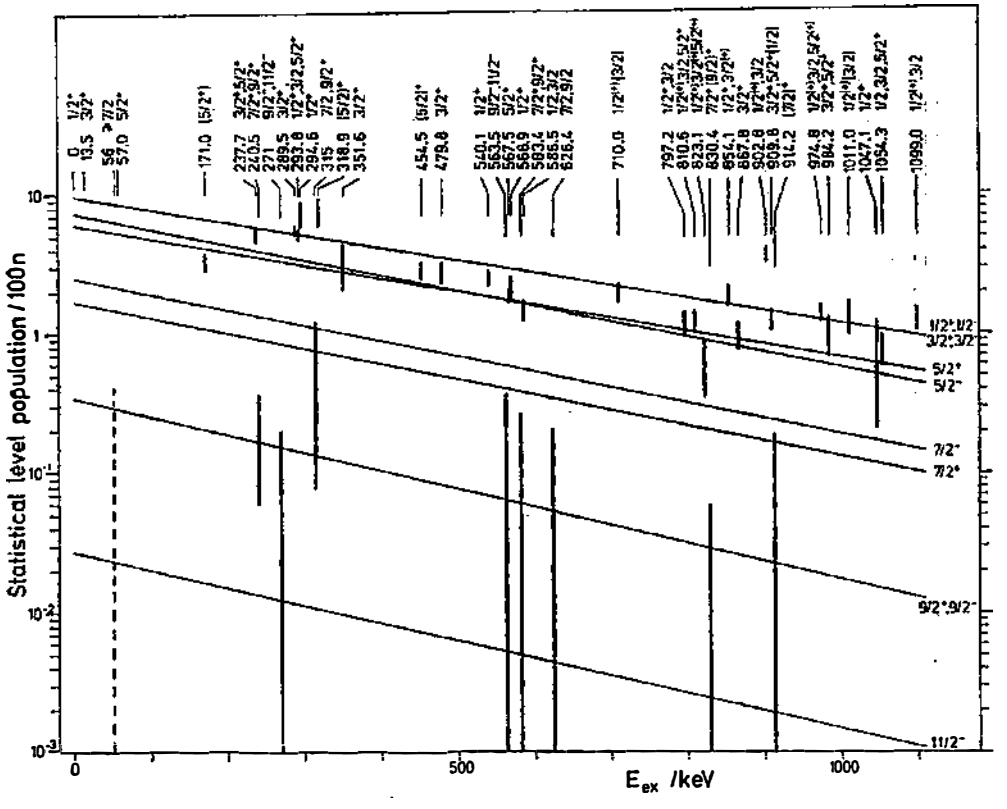

Fig. 9. Experimental (vertical bars) and calculated (sloping lines) statistical population of the low-lying ^{101}Mo states for thermal neutron capture in ^{100}Mo. The experimental values have been derived as difference between the total intensity of transitions depopulating a level and the total intensity of transitions populating the level from the known states with $E_{ex} \leq 1447.2$ keV and the capture state. The exclusion of these discrete transitions reduces the influence of nuclear structure effects.

72.810(5) keV for Pb Kα_2 and 74.968(5) keV for Pb Kα_1 agree very well with the revised values[41] of 17.443, 72.806 and 74.971 keV, respectively, which excludes a systematic error outside the total fitting errors given in Table 2.

The completeness of the level schemes of Figs. 7 and 8 can be estimated from the total ground state population with the use of the absolute capture γ-ray intensities. The γ intensities of transitions feeding the ground state from the 171.0 keV to 1447.3 keV states sum up to 18.4(12)/100 n. The 13.5 keV state (total population from these states 39.7(9)/100 n) and the 57.0 keV state (total population from these states 30.5(11)/100 n) feed the ground state, too, which yields the total ground-state population as 88.6(18)/100 n. The missing intensity can be ascribed to the statistical population of the ground-, 13.5 and 57.0 keV states (calculated values of Fig. 9).

For most of the states the data of Table 4 demonstate how the spin and parity assignments result. A number of states need additional comments.

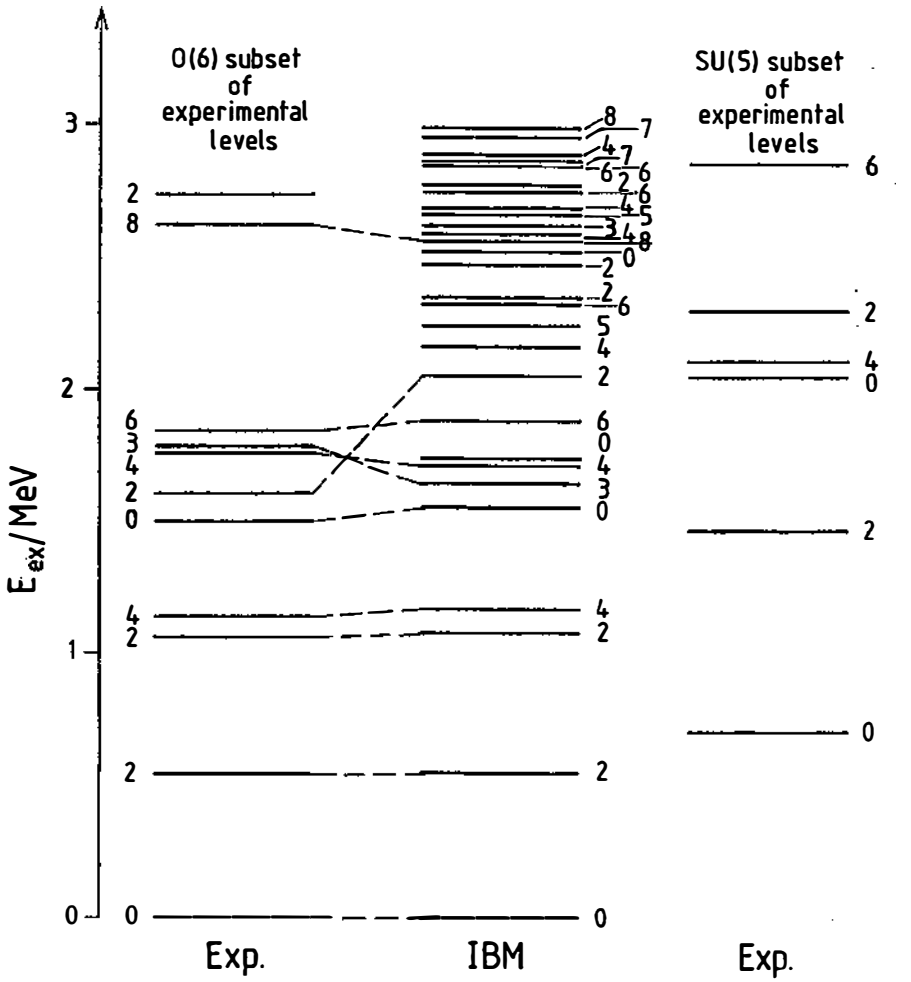

Fig. 10. IBM spectrum of the core. The calculated levels are fitted to the O (6) subsets of experimental levels in ^{100}Mo. The grouping of the levels into the O (6) and SU (5) subsets follows Ref. 55 and preliminary data from Ref. 56.

13.5 keV *and* 57.0 keV *states*: The time-distribution studies at JOSEF and LOHENGRIN[94] yield an average value of $T_{1/2} = 226(7)$ ns for the 13.5 keV state. Its total population in the (n, γ) reaction is 84.6(38)/100 n, including that from the 57.0 keV state and the statistical population (calculated as 9(3)/100 n according to Fig. 9). This value and the γ-ray intensity of 7.8(29)/100 n yield the total conversion coefficients of the 13.5 keV transition to the $1/2^+$ ground-state as 9.8(41). Comparison with the total conversion coefficients α_t (M1) = 11.6, α_t (E2) = 2750, α_t (E1) = 5.30 and α_t (M2) = 2360[42] yields almost pure M1 or E1 character for the 13.5 keV transition with a possible small E2 or M2 admixture of $\leq 8 \cdot 10^{-4}$ and $\leq 4 \cdot 10^{-3}$, respectively[14].

For the 57.0 keV state the transfer-reaction studies yield $J^\pi = 5/2^+$[7,9]. The measurements at JOSEF and LOHENGRIN result in an average value of $T_{1/2} = 133(7)$ ns for this state[14]. Its total population including the calculated statistical population of 5.4(18)/100 n is 35.9(21)/100 n. From the (n,γ) singles spectra the upper limit for the γ intensity of a possible (E2) ground state transition besides the 56.892(20) keV line results as ≤ 0.02/100 n. With the total E2 conversion coefficient of 9.11 the total 57.0 keV transition intensity is ≤ 0.2/100 n. Neglecting this branch, the total population of the 57.0 keV state and the γ-ray intensity of the 43.5 keV transition of 2.37(16)/100 n yield the total conversion coefficient of this transition as 14.1(13). The total conversion coefficents α_t(M1) = 2.77, α_t(E2) = 23.9, α_t(E1) = 1.38 and α_t(M2) = 62.4[42] yield the E2 or M2 component in the 43.5 keV transition as 53(10)% and 21(3)%, respectively, in good agreement with 60(30)% and 17(8)% from the study at JOSEF[14].

As is discussed in Ref. 14, the half-life of the 57.0 keV $5/2^+$ state, the quadrupole/dipole mixing ratio of the 43.5 keV transition, and the dipole character of the 13.5 keV transition to the $1/2^+$ ground-state allow only $J^\pi = 3/2^+$ for the 13.5 keV state. The 43.5 keV $5/2^+ \rightarrow 3/2^+$ γ-transition contains a strong E2 component of 54(9)%, the partial γ-transition probabilities are $P_\gamma(M1) = 1.6(3) \cdot 10^5\ s^{-1}$ and $P_\gamma(E2) = 1.9(4) \cdot 10^4\ s^{-1}$ or $6.3(10) \cdot 10^{-5}$ and 34(8) Weisskopf units (W. u.), respectively. The 13.5 keV $3/2^+ \rightarrow 1/2^+$ ground-state transition is of almost pure M1 character with $P_\gamma(M1) = 2.25(18) \cdot 10^5\ s^{-1}$, corresponding to $3 \cdot 10^{-3}$ W. u., and a possible small $E2$ admixture of $\leq 8 \cdot 10^{-4}$.

The possibility of an additional state at $E_{ex} \approx 56$ keV near to the 57.0 keV level is dicussed in Ref. 14. The fact that in the proton spectrum from the (d, p) reaction the 57 keV peak shows a slight broadening for angles $\geq 30°$ only, would indicate $l_n > 2$ with $l_n = 4$ or 5 being favoured (cf. Fig. 6a). No lines in the (n, γ) spectrum were found which could correspond to transitions depopulating the

TABLE 5.

l_n	J^π	Statistical level population[a] /100 n	Radiation character $J^\pi \rightarrow 3/2^+$	Total conversion coefficient[b]	I_{tot}[c]/100 n	$T^{wk}_{1/2}$[d]/s
3	$5/2^-$	7	E1	1.47	$\leq$ 0.5	$1.7 \cdot 10^{-12}$
	$7/2^-$	2.5	M2	68.4	$\leq$ 13.9	$1.5 \cdot 10^{-4}$
4	$7/2^+$	2	E2	26.0	$\leq$ 5.4	$5.3 \cdot 10^{-6}$
	$9/2^+$	0.3	M3	1250	$\leq$ 250	$4.3 \cdot 10^{2}$
5	$9/2^-$	0.3	E3	774	$\leq$ 155	$1.0 \cdot 10^{1}$
	$11/2^-$	0.03	M4	7310	$\leq$1462	$6.2 \cdot 10^{9}$

[a] From Fig. 9.

[b] α_{tot} from Ref. 42.

[c] Total intensity $I_{tot} = I_\gamma(1 + \alpha_{tot})$.

[d] Weisskopf estimate including internal conversion.

Decay properties of the questionable level at 56 keV calculated for different neutron angular momenta and with the experimental limit of $I_\gamma \leq 0.2$/100 n for the 42.5 keV transition to the 13.5 keV $3/2^+$ state.

possible additional state (the upper γ-ray intensity limits for $\approx$ 42.5 and $\approx$ 56 keV transitions are 0.2/100 n and 0.05/100 n, respectively). The population of a low-lying state with spin J from the higher-lying states in the quasi-continuum according to Fig. 9 is calculated as $\approx$ 9/100 n for $J = 3/2$ and $\approx$ 7/100 n for $J = 5/2$. These numbers for the statistical level population, being lower limits for the total population of a state, should lead to an observable γ depopulation. Thus the missing γ-transition intensity would favour a high spin $J \geq 7/2$ for the possible $\approx$ 56 keV state in agreement with the (d, p) data. For $J \geq 7/2$ this level should be isomeric (cf. Table 5). A search for a $\approx$ 42.5 or 56 keV delayed transition has been performed by taking γ-ray spectra after shutting the neutron beam. No evidence could be found as yet for half-lives in the order of minutes to hours. Thus at present the existence of an additional $\approx$ 56 keV level stays unproven.

237.7 *and* 240.5 keV *states*: The present high-resolution (d, p) reaction study resolves a doublet at 237.8 keV ($l_n = 2$) and 240.5 keV ($l_n = 4$). Only for first state the population and depopulation is established through the data from ^{101}Nb β^- decay and the (n, γ) reaction. For the level at 240.5(10) keV the (n, γ) singles spectra allow a weak transition of 182.1(5) keV and $I_\gamma = 0.11(5)/100$ n to the 57.0 keV $5/2^+$ state. For the transitions to the 13.5 keV $3/2^+$ state and the 171.0 keV $(5/2^+)$ state only upper limits of 0.07/100 n and 0.06/100 n, respectively, can be deduced. The total depopulating intensity of $\leq$ 0.36/100 n including internal conversion is compatible with $J^\pi = 7/2^+$ or $9/2^+$ (Fig. 9).

293.8 *and* 294.6 keV *states*: In the ^{101}Nb β^- decay only the lower state of this doublet is populated. Preliminary results of the (n, γ) study[10] only contained its upper member. However, the γ-γ coincidence intensity ratios of Fig. 4 clearly show the existence of both states. The high-resolution (d, p) study shows that the peak at 295.0(5) keV is mainly excited with $l_n = 0$. Therefore, $J^\pi = 1/2^+$ is assigned to the 294.6 keV state. The observed intensities of the indirect coincidences between the 180.7 keV transition depopulating the 237.7 keV $3/2^+$ or $5/2^+$ state and the transitions feeding the 294.6 keV $1/2^+$ state are higher then expected according to the γ-ray singles intensities of the weak intermediate 56.9 keV transition. This finding can be explained by internal conversion of the 56.9 keV transition. The measured coincidence intensity ratios (e. g. that of Fig. 5b taking into account the coincidence detection efficiency) yield $\alpha_t = 7(2)$. This value indicates $E2$ character for the 56.9 keV transition ($\alpha_t(M1) = 1.27$, $\alpha_t(E2) = 9.18$)[42] and thus allows $J^\pi = 5/2^+$ for the 237.7 keV state.

315 *and* 318.9 keV *states*: The present (d, p)-reaction study reveals a weakly excited state at 315(3) keV with $l_n = 3$ or 4. It might be identical with 318.9 keV state from the γ-spectroscopic investigations. Then the high statistical population of this state (Fig. 9) would only allow $J^\pi = 5/2^-$. Strong coincidence peaks are observed between the 584.0 and 972.6 keV transitions populating the 318.9 keV state and the depopulating transitions of 81.1 and 305.4 keV. For both populating transitions the coincidence intensity ratio (corrected for detection efficiency) of 0.56(6) agrees well with the singles intensity ratio $I_\gamma(81.1)/I_\gamma(305.4) = 0.54(6)$. However, for the 584.0 keV and the 972.6 keV transition the indirect coincidences with the 180.7 keV transition are by a factor 2.22(24) stronger than those with the 81.1 keV transition. The higher intensity of the indirect coincidence must be explained by internal conversion of the intermediate 81.1 keV transition between the 318.9 keV

level and the $3/2^+$ or $5/2^+$ state at 237.7 keV, because no additional transitions have been found which could connect these states. Regarding the decay pattern of the 237.7 keV state under assumption of pure $M1$ character for the 180.7, 223.9 and 238.0 keV transitions, the total conversion coefficient of the 81.1 keV transition results as $\alpha_t = 1.34(26)$. Use of the theoretical conversion coefficients $\alpha_t(M1) = 0.46$, $\alpha_t(E2) = 2.58$, $\alpha_t(E1) = 0.23$ and $\alpha_t(M2) = 5.74$[42] yields 42(13)% $E2$ in the 81.1 $M1/E2$ transition for positive parity of the 318.9 keV state or 20(5)% $M2$ admixture for $E1/M2$ character and negative parity. Such a high $M2$ admixture would result in a μs half-life of the state which contradicts the observation of unattenuated prompt coincidences in the time window of 60 ns. Therefore, the 81.1 keV transition is of $M1 + E2$ character and the spin of the 318.9 keV state ($\pi = +$) must differ from that of the 237.7 keV $3/2^+$ or $5/2^+$ state by at most one unit with $7/2^+$ being excluded according to the high experimental value for the statistical population. This conclusion is in agreement with the results of the resonance capture study[8] which suggests $J^\pi = (5/2)^+$ for the 318.9 keV state.

For the additional $l_n = 3$ or 4 state at 315(3) keV the weak (n, γ) line of 143.1(1) keV and $I_\gamma = 0.12(4)/100$ n may correspond to the transition to the 171.0 keV $(5/2^+)$ state. For the additional possible transitions to the lower-lying $3/2^+$, $5/2^+$ and $7/2^+$ states at 13.5, 57.0, 237.7, 240.5, 289.5, and 293.8 keV only upper I_γ limits of 0.03, 0.08, 0.02, 0.07, 0.04 and 0.05/100 n, respectively, can be deduced. The total depopulating intensity including internal conversion of $\leq 1.2/100$ n is too low to counterbalance the lower limit given by the statistical population of a $5/2^-$ state (Fig. 9). Therefore $J^\pi = 7/2^-$, $7/2^+$ or $9/2^+$ has to be assigned to this state.

454.5 keV *state*: The present (d, p)-reaction experiment yields a clear $l_n = 2$ proton angular distribution (Fig. 6b) and excludes the tentative $1/2^+$ assignment of Refs. 7 and 9. For $l_n = 2$ the data from the ^{100}Mo $(\vec{t},d)$ experiment[9] would favour $J^\pi = 5/2^+$. The study of the γ radiation from resonance neutron capture in ^{100}Mo[8] gives $3/2^+$ for this state according to the primary (dipole) transition to this level in the 1068.2 eV p-wave resonance to which $J^\pi = 1/2^-$ is assigned in Ref. 8. However, as is discussed in Ref. 14, for this resonance $J^\pi = 3/2^-$ cannot be excluded definitely and thus the resonance neutron capture data allow $J^\pi = 3/2^+$ and $5/2^+$ for the $l_n = 2$ 454.5 keV state in agreement with $J^\pi = 5/2^+$ favoured by the $(\vec{t}, d)$ measurement.

563.5, 567.5 *and* 568.9 keV *states*: A primary transition of 4832.6(10) keV in the 97.2 eV $3/2^-$ neutron resonance suggests a state at 565.8(10) keV which is depopulated by a 567.8(5) keV ground-state transition and possibly by a 555.1(5) keV transition which can be placed twice in the level scheme[8]. In thermal neutron capture a primary transition of 4829.5(2) keV from the $1/2^+$ capture state populates a state at 568.8(2) keV. It is observed in coincidence with the 555.3 keV transition, whereas no coincidence with the 567.4 keV transition is found. Thus two near-lying states must exist. Both are confirmed by secondary transitions. With the assumption of dipole character for the primary transitions, the 567.5 keV state (primary transition from the $3/2^-$ resonance capture state) has $J = 1/2$, $3/2$ or $5/2$, whereas the 568.9 keV state only can have $J = 1/2$ or $3/2$. With these two excitation energies the proton angular distribution of the present high-resolution (d, p) study reveals three components in the complex peak around 566 keV: 563.5 keV

with $l_n = 5$, 567.6 keV with $l_n = 2$ and 568.9 keV with $l_n = 0$ (i. e. $J^\pi = 1/2^+$). In the present (n, γ) study only one weak transition of 392.9 keV with $I_\gamma = 0.25(14)$/100 n was found which could depopulate the 563.5(10) keV state. This transition can also be placed between the 1447.3 and 1054.3 keV states (Fig. 8). The low experimental upper limit for the total population of the 563.5 keV state (Fig. 9) supports the high spin assignment of $9/2^-$ or $11/2^-$. The level energies given in Ref. 9 lie systematically by 2—3 keV lower than those of the present work. Therefore, the 564 keV $l_n = 2$ peak of Refs. 7 and 9 corresponds very likely to the 567.5 keV state of the present work. Then for this state the polarization asymmetry[9] yields $J^\pi = 5/2^+$.

583.4 *and* 586.5 keV *states*: The earlier neutron-stripping reaction studies[7,9] and the present (d, p) measurement yield an $l_n = 4$ state, i. e. $J^\pi = 7/2^+$ or $9/2^+$, at 583.4 keV. Its high spin value is compatible with the 412.1 keV transition to the $(5/2^+)$ state at 171.0 keV. The weak 4813(3) keV primary transition in the 364 eV $1/2^+$ resonance[8] yields a level at 585(3) keV which has $J = 1/2$ or 3/2, if dipole character of the primary transition is assumed. The present study leads to a state at 586.5 keV which is depopulated by two transitions to states with $J^\pi = 1/2^+$. Their total intensity is compatible with a low spin value of the 586.4 keV state (Fig. 9) which therefore should correspond to the state populated in resonance neutron capture.

626.4, 830.4, 914.2 *and* 1447.3 keV *states*: The low experimental statistical population (Fig. 9) and the fact that no primary transition is observed in any 1/2 and 3/2 neutron resonance[8] favour $J \geq 7/2$ for the first three states. Assumption of dipole or quadrupole character for the 388.6 keV transition between the 626.4 keV state and the 237.7 keV $J^\pi = 3/2^+$ or $5/2^+$ state only allows $J = 7/2$ or 9/2 for the 626.4 keV state. For the 830.4 and 914.2 keV states the assignment $J \geq 7/2$ is in agreement with $l_n = 4$, i. e. $J^\pi = 7/2^+$ or $9/2^+$[7,9]. For the 914.2 keV state the ^{100}Mo $(\vec{t}, d)$ measurement[9] favours $J^\pi = 7/2^+$ which is compatible with the transitions populating and depopulating this state (Figs. 7, 8). For the 1447.3 keV state the strong primary (dipole) transitions in thermal and $1/2^+$ 364 eV resonance neutron capture[8] only allow $J = 1/2$ or 3/2. The 616.8 keV transition to the 830.4 keV state with $J^\pi = 7/2^+$ or $9/2^+$ which is too weak to the observed in coincidence would only allow $J^\pi = 7/2^+$ for the 830.4 keV and $J^\pi = 3/2^+$ for the 1447.3 keV state, if $M2$ character for this transition is excluded according to the γ-decay pattern of the 1447.3 keV state.

4. *Theoretical description*

The calculations for ^{101}Mo were performed in the framework of the SU(6) symmetry by coupling a neutron quasiparticle in the $N = 50 - 82$ shell to the $^{100}_{42}Mo_{58}$ core. The even-even core nucleus ^{100}Mo is described in the interacting boson model IBM[43]/TQM[44,45] and the odd-even nucleus ^{101}Mo in the interacting boson-fermion model IBFM[46]/PTQM[45,47]. The calculations use the TQM representation of IBM with the Hamiltonian given by the equations 5 and 9—13 of Ref. 47.

It should be noted that the available experimental data put very stringent requirements on the theoretical description of this nucleus. In ^{101}Mo there is a pronounced low-lying triplet of states with $J^\pi = 1/2^+$ (g. s.), $3/2^+$ at 13.5 keV and $5/2^+$ at 57.0 keV. These three states are characterized by four experimental features:

$$I_\gamma(5/2_1^+ \to 1/2^+)/I_\gamma(5/2_1^+ \to 3/2_1^+) \leq 0.008. \tag{1a}$$

54(9)% $E2$ admixture in the $5/2_1^+ \to 3/2_1^+$ transition. (1b)

The $3/2_1^+ \to 1/2_1^+$ $M1$ transition is strongly hindered

($P_\gamma(M1) = 2.25(18) \cdot 10^5\,\mathrm{s}^{-1}$ or $3 \cdot 10^{-3}$ Weisskopf units)

and the $E2$ admixture is small ($\leq 8 \cdot 10^{-4}$). (1c)

For the spectroscopic factors the transfer data of

Table 4 yield $S_{d,p}(1/2^+) \approx S_{d,p}(5/2^+) \gg S_{d,p}(3/2_1^+)$. (1d)

The experimental feature (1d) excludes the interpretation of the $3/2^+$ member of the low-lying triplet as the $\tilde{d}_{3/2}$ quasiparticle state. This is in accordance with the observation that the $\tilde{d}_{3/2}$ quasiparticle state is not close[16] to the Fermi surface in this mass region.

Next we note that the features (1a, b, d) also exclude the possibility to interpret the low-lying triplet in ^{101}Mo as the IBFM anomalous triplet of states $J = j = 5/2$, $J = j - 1 = 3/2$, $J = j - 2 = 1/2$, associated with a $\tilde{d}^3_{5/2}$ quasiparticle configuration. A first calculation on ^{101}Mo along this line of $J = j - 2$ parametrization was performed[48] similar to those for the heavier $N = 59$ isotones ^{105}Pd[49] and ^{103}Ru[50]. As for these cases the $\tilde{d}_{5/2}$ quasiparticle is the lowest-lying one. However, in the present calculation somewhat stronger boson-fermion interaction strengths have been used. In this picture the $1/2_1$, $3/2_1$ and $5/2_1$ states have $|\tilde{d}_{5/2}, 12; 1/2\rangle$, $|\tilde{d}_{5/2}, 12; 3/2\rangle$ and $|\tilde{d}_{5/2}, 00; 5/2\rangle$, respectively, as the largest component with small admixtures arising from the other quasiparticle states. Such a pattern, refferred to as $J = j - 1$, $j - 2$ anomaly, was previously studied in the frame of IBFM and of the cluster-vibration model[51-53].

The electromagnetic properties associated with the $J = j - 2$ parametrization would be as follows. Employing the effective charges from the ^{103}Ru calculation[50] and standard gyromagnetic ratios ($g_R = Z/A$, $g_l = g_l^{\nu free} = 0$, $g_s =$, $= 0.7 g_s^{\nu free}$), the reduced probabilities for the $3/2_1 \to 1/2_1$ transition are[48]: $B(E2, 3/2_1 \to 1/2_1) = 0.0028\, e^2b^2$, and $B(M1, 3/2_1 \to 1/2_1) = 0.0034\, \mu_N^2$. They result in $P_\gamma(E2) = 1.54 \cdot 10^1\,\mathrm{s}^{-1}$, $P_\gamma(M1) = 1.49 \cdot 10^5\,\mathrm{s}^{-1}$ for the 13.5 keV ground-state transition or $T_{1/2} = 340$ ns for the 13.5 keV level in rather good agreement with the experimental values of $P_\gamma(E2) \leq 2.4 \cdot 10^2\,\mathrm{s}^{-1}$ and $P_\gamma(M1) = 2.25(18) \cdot 10^5\,\mathrm{s}^{-1}$ as deduced from the total conversion coefficient and the measured value $T_{1/2} = 226(7)$ ns. However, for the depopulation of the second excited state the results in the $J = j - 2$ parametrization are: $B(E2, 5/2_1 \to 3/2_1) = 0.0001\, e^2b^2$, $B(E2, 5/2_1 \to 1/2_1) = 0.047\, e^2b^2$, $B(M1, 5/2_1 \to 3/2_1) = 0.0007\, \mu_N^2$. Thus the $J = j - 2$ parametrization predicts:

a) $I_\gamma(5/2_1^+ \to 1/2_1^+)/I_\gamma(5/2_1^+ \to 3/2_1^+) = 0.34$,

b) 0.1% $E2$ admixture in the $5/2_1^+ \to 3/2_1^+$ transition

in contradiction to the experimental data (1a, b). This discrepancy is a persistent feature of the $\tilde{d}^3_{5/2}$ pattern rather insensitive to details of parametrization. In addition, the $J = j - 2$ parametrization predicts a small spectroscopic factor for the $1/2_1$ ground state in contradiction to the experiment (1d).

Thus, realistic calculations on ^{101}Mo must follow a different line. Let us first construct the zeroth-order approximation for the structure of the lowest-lying triplet of levels which accomodates the features (1a—d). A natural choice is

$$|1/2_1\rangle_0 = |\tilde{s}_{1/2}\rangle \tag{2a}$$

$$|3/2_1\rangle_0 = |\tilde{d}_{5/2}, 12; 3/2\rangle \tag{2b}$$

$$|5/2_1\rangle_0 = |\tilde{d}_{5/2}\rangle \tag{2c}$$

with the $\tilde{s}_{1/2}$ and $\tilde{d}_{5/2}$ quasiparticle states being nearly half-filled, i. e.

$$v(\tilde{s}_{1/2}) \approx u(\tilde{s}_{1/2}) \quad \text{and} \tag{3a}$$

$$v(\tilde{d}_{5/2}) \approx u(\tilde{d}_{5/2}) \tag{3b}$$

in accordance with the experimental neutron-transfer data[34,35]. Here, the IBFM basis states are denoted by

$$|\tilde{j}, n_d I; J\rangle, \tag{4}$$

where the quasiparticle state $\tilde{j}$ and the boson state with n_d d-bosons of angular momentum I are coupled to the total angular momentum J. Thus, in the zeroth order we assign the $3/2_1$ state to a d-boson multiplet state involving the $\tilde{d}_{5/2}$ quasiparticle.

Employing the identification (2a—c) we have in the zeroth-order:

$$\text{a) } B(E2, |5/2_1\rangle_0 \to |1/2_1\rangle_0) \sim [u(\tilde{d}_{5/2})\, u(\tilde{s}_{1/2}) - v(\tilde{d}_{5/2})\, v(\tilde{s}_{1/2})]^2 \approx 0. \tag{5}$$

Here we have employed also (3a, b). Thus $I_\gamma(5/2_1 \to 1/2_1) \approx 0$, i. e. the feature (1a) is satisfied

$$\text{b) } B(E2, |5/2_1\rangle_0 \to |3/2_1\rangle_0) \sim B(E2, |12\rangle \to |00\rangle). \tag{6}$$

Thus, the feature (1b) can be satisfied.

$$\text{c) } B(M1, |3/2_1\rangle_0 \to |1/2_1\rangle_0 = 0, \tag{7}$$

since the $M1$ operator does not change the number of d-bosons. Thus, the feature (1c) is satisfied.

$$\text{d) } S_{d,p}(|1/2_1\rangle_0) \approx S_{d,p}(|5/2_1\rangle_0) \approx 0.5, \text{ whereas } S_{d,p}(|3/2_1\rangle_0) = 0, \tag{8}$$

where we have employed also (3a, b). These results satisfy the feature (1d).

In the next step we are using the zeroth-order approximation (2a—c) and (3a, b) as a guideline for our calculation. It immediately follows for the quasiparticle energies that

$$E(\tilde{s}_{1/2}) < E(\tilde{d}_{5/2}) < E(\tilde{d}_{3/2}), E(\tilde{g}_{7/2}). \tag{9}$$

The basis state (2b) can be lowered below the $\tilde{d}_{5/2}$ state as an effect of the $j-1$ anomaly which in IBFM emerges as a consequence of the exchange force[47,51]. If the strength Λ_0 of the exchange force is sizeable and the relation (3b) is satisfied, this lowering will appear.

Let us now turn to the IBM core for the IBFM calculation. The core nucleus ^{100}Mo is rather complex. It has been interpreted as a case of coexisting structures[55] One which includes the ground-state band approximately corresponds to the O(6) limit, whereas the second one corresponds to the SU(5) limit (see Fig. 10). Since we are investigating only the low-lying states of ^{101}Mo, we are fitting the IBM core to the O(6) subset of experimental levels. In this way we obtain the IBM spectrum presented in Fig. 10. The corresponding core parameters are $h_1 = -0.45$, $h_2 = -0.15$, $h_3 = 0.007$, $h_{40} = h_{44} = 0$, $h_{42} = -0.12$ which is a somewhat distorted O(6) type of parametrization. The boson number $N = 6$ corresponds to the valence-shell nucleons outside $Z = 38$, $N = 50$. The IBM wavefunctions of several low-lying states are presented in Table 6. The wave functions are expressed in the sd-boson basis

$$|I\rangle = \sum_{n_d,v} \xi_{n_d,vI} |n_d\, vI\rangle.$$

Here $|n_d vI\rangle$ denotes a state with n_d d-bosons, coupled to the angular momentum I, and with $N - n_d$ s-bosons. The number v is an additional quantum number to distinguish, if needed, between different states of the same n_d and I.

Employing this core parametrization and previous guidelines for the quasiparticle and boson-fermion interaction parameters, we determine the IBFM parametrization in such a way as to get an overall agreement with the ^{101}Mo data. The $\tilde{s}_{1/2}$, $\tilde{d}_{5/2}$, $\tilde{g}_{7/2}$ and $\tilde{d}_{3/2}$ quasiparticle energies and occupation probabilities result as 0, 0.26, 0.56 and 1.0 MeV and 0.50, 0.65, 0.28 and 0.25, respectively. The boson-fermion interaction strengths are $A_0 = 0.1$, $\Gamma_0 = 0.04$ and $\Lambda_0 = 1.0$ MeV. The calculated positive-parity spectrum is presented in Fig. 11 and compared to the available experimental levels. In Table 7 the IBFM wave functions of the 6 lowest-lying calculated states are presented. The wave functions are expressed in the boson-fermion coupled basis

$$|J\rangle = \sum_{j,n_d,v,I} \xi^J_{jn_dvI} |j, n_d\, v\, I; J\rangle.$$

TABLE 6.

0_1		2_1	2_2		4_1
n_dI^a	ξ_{n_dI}	n_dI^a	ξ_{n_dI}	ξ_{n_dI}	n_dI^a	ξ_{n_dI}
00	0.72	12	0.75	0.03	24	0.79
20	−0.63	22	−0.03	0.79	34	−0.04
30	−0.01	32	−0.61	−0.02	44	−0.59
40	0.30	42	0.02	−0.59	44′	0.00
50	0.01	42′	0.01	0.00	54	0.02
60	−0.06	52	0.24	0.00	54′	−0.01
60′	−0.00	52′	−0.00	0.01	64	0.17
		62	−0.01	0.17	64	0.00
		62′	−0.00	−0.00	64″	−0.00

[a] The following notation for the basis states is employed: n_dI denotes the boson state $|n_d v_{lowest} I\rangle$ (the quantum number v is not needed for $n_d < 4$). Otherwise, we abbreviate $|n_d v' I\rangle$ by $|n_d I'\rangle$, where $v' > v_{lowest}$.

Wave-function amplitudes of the 0_1, 2_1, 2_2 and 4_1 states of the boson core.

TABLE 7.

J_r	j, n_dI^a	$\xi^{J_r}_{j,n_dI}$	J_r	j, n_dI^a	$\xi^{J_r}_{j,n_dI}$
$1/2_1$	$s_{1/2}$, 00	0.59	$3/2_2$	$d_{5/2}$, 22	0.48
	$s_{1/2}$, 20	−0.57		$d_{5/2}$, 24	−0.33
	$s_{1/2}$, 40	0.32		$d_{5/2}$, 42	−0.47
	$d_{5/2}$, 22	−0.26		$d_{5/2}$, 44	0.31
	$d_{5/2}$, 42	−0.22		$d_{5/2}$, 62	0.21
	$g_{7/2}$, 24	−0.21		$g_{7/2}$, 24	0.22
				$g_{7/2}$, 44	−0.23
$3/2_1$	$d_{5/2}$, 12	0.60			
	$d_{5/2}$, 32	−0.64	$7/2_1$	$d_{5/2}$, 24	−0.29
	$d_{5/2}$, 52	0.34		$d_{5/2}$, 44	0.28
				$g_{7/2}$, 00	0.44
$5/2_1$	$d_{5/2}$, 00	0.52		$g_{7/2}$, 20	−0.54
	$d_{5/2}$, 20	−0.60		$g_{7/2}$, 24	−0.25
	$d_{5/2}$, 24	−0.23		$g_{7/2}$, 40	0.38
	$d_{5/2}$, 40	0.39		$g_{7/2}$, 44	0.25
	$d_{5/2}$, 44	0.22			
$5/2_2$	$d_{5/2}$, 12	0.36	[a] for notation of the boson states see footnote to Table 6.		
	$d_{5/2}$, 32	−0.38			
	$d_{5/2}$, 52	0.21			
	$g_{7/2}$, 12	0.44			
	$g_{7/2}$, 32	−0.50			
	$g_{7/2}$, 52	0.29			

Wawe function amplitudes of the lowest-lying calculated positive parity states in ^{101}Mo. Only components with amplitudes squared larger than 4% are listed.

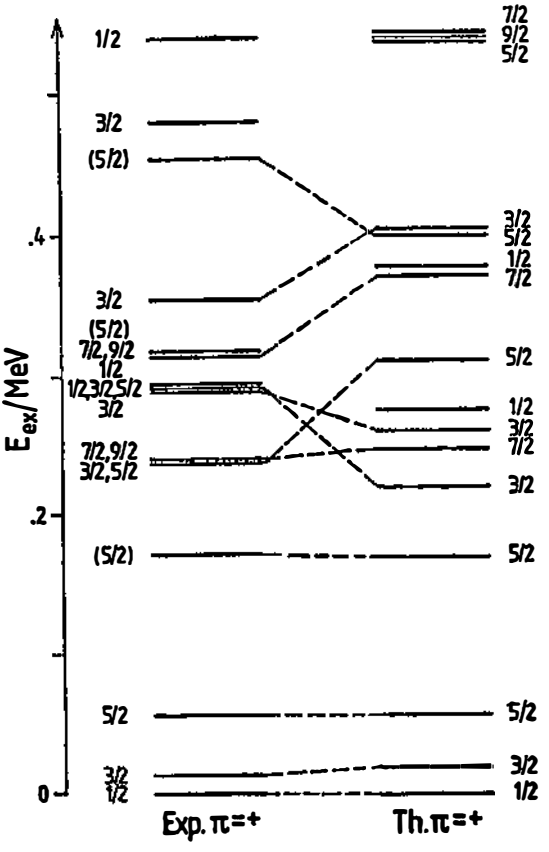

Fig. 11. Calculated low-lying positive-parity states of ^{101}Mo in comparison with the experimental states. The present (d, p) study indicates the possible existence of an additional state at 56 keV with $J \geq 7/2$.

In the basis state $|j, n_d v I; J\rangle$ the quasiparticle j and the n_d-boson state $|n_d v I\rangle$ of angular momentum I are coupled to the total angular momentum J. Employing these wave functions we have calculated the electromagnetic properties of the low lying states using the following effective charges and gyromagnetic ratios: $e^{\nu} = 0.5$, $e^{\nu ib} = 0.9$, $g_R = 0.17$, $g_l = g_l^{\nu free} = 0$, $g_s = 0.7\, g_s^{\nu free} = -2.68$. Here e^{ν}, g_l and g_s have the standard values, while $e^{\nu b}$ and g_R were adjusted to the ^{101}Mo data. In this way the g_R value is reduced from its standard value similarly as in Ref. 47. The IBFM electromagnetic properties, which result from this parametrization, are presented in Tables 8—10. In Table 8 we list the calculated $B(E2)$ and $B(M1)$ values and branching ratios for the transitions between the low-lying positive-parity states in comparison with the experimental data. In Table 9 we present the half-lives of the low-lying states, obtained from the calculated reduced transition probabilities of Table 8 and theoretical internal conversion coefficients. Table 10 contains the calculated electric quadrupole and magnetic dipole moments of the low-lying states. As can be seen from Table 8, the experimental electromagne-

TABLE 8.

Initial state/keV	Transition[a]		B(E2) /$10^{-2}e^2b^2$	B(M1) /$10^{-2}\mu_N^2$	γ-branching ratio calc.	exp.
13.5	$3/2_1$	$\rightarrow 1/2_1$	0.26	0.40	100	100
57.0	$5/2_1$	$\rightarrow 3/2_1$	5.4	0.11	100	100
		$\rightarrow 1/2_1$	0.001	—	0.01	$\leq$0.8
171.0	$(5/2_2)$	$\rightarrow 5/2_1$	1.9	0.002	0.06	6.5(3)
		$\rightarrow 3/2_1$	0.20	11.2	100	100
		$\rightarrow 1/2_1$	0.42	—	0.10	$\leq$0.3
237.7	$(5/2_3)$	$\rightarrow(5/2_2)$	3.7	0.23	0.27	$\leq$0.2
		$\rightarrow 5/2_1$	0.001	4.4	100	100
		$\rightarrow 3/2_1$	1.3	0.17	9.7	3.8(7)
		$\rightarrow 1/2_1$	0.05	—	0.09	1.3(6)
240.5	$(7/2_1)$	$\rightarrow(5/2_2)$	5.1	0.11	0.5	b
		$\rightarrow 5/2_1$	0.02	1.2	100	b
		$\rightarrow 3/2_1$	0.91	—	5.0	b
289.5	$3/2_2$	$\rightarrow(7/2_1)$	0.44	—	0	$\leq$0.1
		$\rightarrow(5/2_3)$	0.37	0.56	1.1	$\leq$0.1
		$\rightarrow(5/2_2)$	0.05	0.24	5.3	10.5(5)
		$\rightarrow 5/2_1$	0.08	0.01	2.7	4.7(5)
		$\rightarrow 3/2_1$	0.30	0.33	100	100
		$\rightarrow 1/2_1$	3.1	0.31	163	11.0(9)
293.8	$(3/2_3)$	$\rightarrow(7/2_1)$	0.04	—	0	$\leq$0.3
		$\rightarrow(5/2_3)$	0	18.7	25	$\leq$0.3
		$\rightarrow(5/2_2)$	1.2	0.24	5	$\leq$1.7
		$\rightarrow 5/2_1$	0.01	0.88	125	34 (3)
		$\rightarrow 3/2_1$	4.0	0.19	100	100
		$\rightarrow 1/2_1$	0.41	1.8	500	55 (2)
315	$(7/2_2)$	$\rightarrow(3/2_3)$	1.50	—	0	b
		$\rightarrow 3/2_2$	0.11	—	0	b
		$\rightarrow(7/2_1)$	0.54	0.007	0.02	b
		$\rightarrow(5/2_3)$	0.25	0.09	0.2	b
		$\rightarrow(5/2_2)$	0.004	6.99	100	b
		$\rightarrow 5/2_1$	5.85	0.04	25.5	b
		$\rightarrow 3/2_1$	0.009	—	0.1	b
351.6	$3/2_4$	$\rightarrow(7/2_2)$	0.22	—	0	1.6(5)[c]
		$\rightarrow 1/2_2$	0.05	0.001	0.00004	$\leq$0.1
		$\rightarrow(3/2_3)$	0.25	15.5	0.6	$\leq$0.1
		$\rightarrow(7/2_1)$	0.02	—	0.00006	$\leq$1.5
		$\rightarrow(5/2_3)$	0.03	5.7	1.7	$\leq$3
		$\rightarrow(5/2_2)$	0.49	0.47	0.6	5.3(14)
		$\rightarrow 5/2_1$	0.01	19.9	100	100
		$\rightarrow 3/2_1$	0.10	0.02	0.2	3.7(9)
		$\rightarrow 1/2_1$	0.006	0.69	5.9	53 (6)

TABLE 8 continued.

Initial state/keV	Transition[a]		$B(E2)$ /$10^{-2}e^2b^2$	$B(M1)$ /$10^{-2}\mu_N^2$	γ-branching ratio calc.	exp.
454.5	$(5/2_4)$	$\rightarrow(7/2_2)$	0.013	7.4	3.3	≤ 1.5
		$\rightarrow 3/2_4$	0.14	0.03	0.005	≤ 0.2
		$\rightarrow 1/2_2$	0.02	—	0	≤ 0.5
		$\rightarrow(3/2_3)$	0.50	1.3	1.0	≤ 0.5
		$\rightarrow(3/2_2)$	0.001	18.8	13.9	1.1(5)
		$\rightarrow(7/2_1)$	1.2	0.1	0.2	≤ 0.4
		$\rightarrow(5/2_3)$	0.02	0.4	0.5	6.2(9)
		$\rightarrow(5/2_2)$	0.007	12.9	47	20.2(9)
		$\rightarrow 5/2_1$	0.49	0.09	1.5	6.4(13)
		$\rightarrow 3/2_1$	0	7.2	100	100
		$\rightarrow 1/2_1$	3.3	0	7.2	8.3(22)

[a] Spin values which do not result unambiguously from the experiments are given within brackets. The sequence of the calculated $3/2_2$ and $3/2_3$ and of the calculated $1/2_2$ and $1/2_3$ states has been interchanged (see text).

[b] Due to the high spin the depopulating transitions are expected to be weak in the (n, γ) reaction and β^- decay. However, with use of the calculated branching ratios a weak line of appropriate energy could be detected in the (n, γ) singles spectra which may correspond to the strongest transition, whereas only upper limits can be given for the additional transitions (see Section 3).

[c] The weak line of 37.0(4) keV may correspond to this transition, see Table 2.

Calculated reduced transition probabilities and branching ratios for low-lying positive parity states in ^{101}Mo compared to the experimental data. For each state the γ-branching ratios are normalized to the strongest experimental transition.

TABLE 9.

Level[a] E/keV	J_π	$T_{1/2}$/ns calc.	exp.
13.5	$3/2_1$	294	226(7)
57.0	$5/2_1$	78	133(7)
171.0	$(5/2_2)$	0.09	
237.7	$(5/2_3)$	0.14	
240.5	$(7/2_1)$	0.53	
289.5	$3/2_2$	0.19	

[a] See footnote a to Table 8.

Calculated half-lives of the low-lying positive-parity states in comparison with the experimental data.

tic intensity rules (1a—c) for the low-lying triplet are well reproduced by the calculated results:

a) $I_\gamma(5/2_1 \rightarrow 1/2_1)/I_\gamma(5/2_1 \rightarrow 3/2_1) = 10^{-4}$.

b) $B(E2, 5/2_1 \rightarrow 3/2_1)$ is large, $B(M1, 5/2_1 \rightarrow 3/2_1)$ is small, yielding an $E2$ component of 6% in the $5/2_1 \rightarrow 3/2_1$ transition.

c) $B(M1, 3/2_1 \rightarrow 1/2_1)$ is 10^{-3} times the Weisskopf estimate and the $E2/M1$ mixing ratio calculated from the $B(E2)$ and $B(M1)$ values of Table 8 is $8 \cdot 10^{-5}$.

TABLE 10.

E/keV	Level[a] J_r	Q/eb	μ/μ_N
0.0	$1/2_1$	—	−1.15
13.5	$3/2_1$	0.03	−0.58
57.0	$5/2_1$	0.06	−1.01
171.0	$(5/2_2)$	0.09	0.18
237.7	$(5/2_3)$	−0.13	0.46
240.5	$(7/2_1)$	−0.04	0.85
289.5	$3/2_2$	−0.07	0.76

[a] See footnote a to Table 8.

Static moments of the low-lying positive-parity states of ^{101}Mo calculated in IBFM.

The rule (1d) for the spectroscopic factors is also satisfied, because the calculated amplitudes of the $\tilde{s}_{1/2}$ and $\tilde{d}_{5/2}$ components in the wave functions of the $1/2_1$ and $5/2_1$ states are sizeable (amounting to 0.59 and 0.52, respectively), while the amplitude for $\tilde{d}_{3/2}$ component in the wave function of the $3/2_1$ state is very small (<0.01).

As is finally seen from Table 9, the IBFM calculation yields the half-lives of the 13.5 and 57.0 keV levels in rather good agreement with the experimental values.

5. *Discussion*

Let us now discuss the structure of IBFM wave functions of ^{101}Mo. It turns out that we can group the components into blocks which approximately resemble the d-boson structure of the core. For example, the components which involve the $\tilde{s}_{1/2}$ quasiparticle in the $|1/2_1\rangle$ wave functions can be approximately presented as one block:

$$0.59\,|\tilde{s}_{1/2}, 00; 1/2\rangle - 0.57\,|\tilde{s}_{1/2}, 20; 1/2\rangle - 0.02\,|\tilde{s}_{1/2}, 30; 1/2\rangle +$$

$$+ 0.32\,|\tilde{s}_{1/2}, 40; 1/2\rangle + 0.01\,|\tilde{s}_{1/2}, 50; 1/2\rangle - 0.09\,|\tilde{s}_{1/2}, 60; 1/2\rangle \approx$$

$$\approx 0.87\,|\tilde{s}_{1/2}, 0_1; 1/2\rangle. \tag{10}$$

In the basis vector $|\tilde{s}_{1/2}, 0_1; 1/2\rangle$ on the right-hand side, 0_1 denotes the wave function of the ground state of the boson core as presented in Table 6. In general, the IBFM vectors

$$|\tilde{j}, I_r; J\rangle \tag{11}$$

form the basis which is referred to as truncated weak-coupling (TWC) basis[53]. There I_r denotes the wave function of the boson core for the r-th state of angular momentum I.

It turns out that the IBFM wave functions of the low-lying states of ^{101}Mo exhibit a much simpler structure when transformed from the boson-fermion basis (4) to the TWC basis (11). By performing such a transformation for the three lowest states of ^{101}Mo, we observe that the wave function of each state is dominated by one TWC basis state, namely

$$|1/2_1\rangle = 0.87\,|\tilde{s}_{1/2}, 0_1; 1/2\rangle + \ldots \tag{12a}$$

$$|3/2_1\rangle = 0.93\,|\tilde{d}_{5/2}, 2_1; 3/2\rangle + \ldots \tag{12b}$$

$$|5/2_1\rangle = 0.86\,|\tilde{d}_{5/2}, 0_1; 5/2\rangle + \ldots \tag{12c}$$

This explains, why the features (5)—(8) of the zeroth-order approximation are qualitatively preserved in the IBFM calculation in spite of sizeable interaction strengths.

In particular, let us discuss the spectroscopic factors of the $1/2_1$ and $5/2_1$ states employing the leading terms in (12a) and (12c). In this way, the spectroscopic factors associated with the $0_1 \to 1/2_1$ and $0_1 \to 5/2_1$ one-particle transfer are:

$$S_{d,p}(1/2_1) = u(\tilde{s}_{1/2})^2 \cdot \langle s_{1/2}, 0_1; 1/2|1/2_1\rangle^2 = 0.50 \cdot 0.87^2 = 0.38 \text{ and}$$

$$S_{d,p}(5/2_1) = u(\tilde{d}_{5/2})^2 \cdot \langle \tilde{d}_{5/2}, 0_1; 5/2|5/2_1\rangle^2 = 0.35 \cdot 0.86^2 = 0.26.$$

These values have to be compared with the experimental results which according to Table 4 are 0.18 and 0.07, respectively. Qualitative agreement is found for the $1/2_1$ state, whereas for the $5/2_1$ state the zeroth order approximation underestimates the phonon admixed components in the $|5/2_1\rangle$ wave function.

It is interesting to note that the $5/2_2$ state has two sizeable components when transformed to the TWC basis:

$$|5/2_2\rangle = 0.56\,|\tilde{d}_{5/2}, 2_2; 5/2\rangle + 0.68\,|\tilde{g}_{7/2}, 2_1; 5/2\rangle + \ldots \tag{12d}$$

Employing the TWC forms (12b, c) we get

$$B(M1, 5/2_2 \to 3/2_1) \approx B(M1, |\tilde{d}_{5/2}, 2_2; 5/2\rangle \to |\tilde{d}_{5/2}, 2_1; 3/2\rangle) \approx$$

$$\approx B(M1, 2_2 \to 2_1) \quad \text{and}$$

$$B(M1, 5/2_2 \to 5/2_1) \approx B(M1, |\tilde{d}_{5/2}, 2_2; 5/2\rangle \to |\tilde{d}_{5/2}, 0_1; 5/2\rangle) = 0$$

and thus

$$B(M1, 5/2_2 \to 3/2_1) \gg B(M1, 5/2_2 \to 5/2_1)$$

in agreement with the IBFM values of Table 8 and with the experimental branching ratios.

The nature of the low-lying triplet of states is also reflected in the calculated static moments. Thus, the calculated magnetic dipole moments of the states $1/2_1$, $3/2_1$ and $5/2_1$ reflect the signs associated with a quasiparticle in the dominant TWC component, i. e. with $\tilde{s}_{1/2}$, $\tilde{d}_{5/2}$ and $\tilde{d}_{5/2}$, respectively. These predictions are preserved by the boson-fermion interaction due to the mechanism investigated in Ref. 57.

Let us comment on two possible problems in comparing the calculated levels and the experimental data. The first is connected with the 294.6 keV $1/2^+$ level. This level cannot be unambigously assigned to the theoretical $1/2_2$ or the $1/2_3$ state. The experimental γ-branching ratios to the $(5/2_3)$, $(5/2_2)$, $5/2_1$, $3/2_1$, $1/2_1$ states are $1.4(2)/\leq 0.6/100/48(2)/46(3)$. For the calculated $1/2_2^+$ state the corresponding branching ratios are 0.05/0.01/100/315430/2770, while for the calculated $1/2_3^+$ level they are 10/10/100/950/4050. In both cases the calculated γ-branches to the $3/2_1$ and $1/2_1$ states are by far too strong. The decay of the $3/2_4$ state at 351.6 keV and the $5/2_4$ state at 454.5 keV to the 294.6 keV level is not a sensitive test. The relative experimental γ-branchings (Table 7) are ≤ 0.1 and ≤ 0.5, respectively. For the $1/2_3^+$ assignment to the 294.6 keV state (as adopted in Table 7) the calculated values are 0.00004 and 0.0002, while for $1/2_2^+$ they are 0.006 and 0.00002, respectively. Both assignments are consistent with the experiment.

For the assignment $1/2_2^+$ to the 294.6 keV level, where the highest discrepancy is encountered in the transition to the $3/2_1$ state, the high calculated value is due to the large $B(M1, 1/2_2 \rightarrow 3/2_1)$ value of 0.813 μ_N^2. This value is rather stable against changes in the parametrization. It seems rather improbable that it could be reduced by the necessary 4 orders of magnitude by admixtures not contained in the model. Therefore it is concluded that the theoretical counterpart of the 294.6 keV $1/2^+$ level is not the calculated $1/2_2^+$ state. Thus a possible candidate in the framework of the present calculation is the $1/2_3^+$ state. The theoretical γ-branching ratios in this case are governed by rather small reduced transition probabilities: $B(E2, 1/2_3 \rightarrow 5/2_1) = 0.0004\, e^2b^2$, $B(E2, 1/2_3 \rightarrow 3/2_1) = 0.0001\, e^2b^2$, $B(M1, 1/2_3 \rightarrow 3/2_1) = 0.0001\, \mu_N^2$ and $B(M1, 1/2_3 \rightarrow 1/2_1) = 0.0004\, \mu_N^2$. These values can be strongly influenced by non-model admixtures in the wave functions which can be the consequence of coupling to the SU(5) subset of core states. Due to the quasiparticle positions this coupling should strongly influence the $1/2^+$ states and may shift the $1/2_2^+$ state (decaying almost exclusively to the $3/2_1^+$ state) upwards in energy. Unfortunately, calculations for odd-A nuclei with two different coupling structures in the core are not available at present.

The second possible problem is connected with the possible state at 56 keV ($J \geq 7/2$). This state (if it exists and has positive parity) is outside the IBFM model space, i. e. its nature is different from that of the other low-lying positive parity states. This assumption is supported by the fact that no γ transition from the established levels to this state has been observed in the present studies. For negative parity the assignments $J^\pi = 7/2^-$ and $9/2^-$ would imply an appreciable deformation. In these cases as well as for the alternative $J^\pi = 11/2^-$ the questionable 56 keV state should be an isomer for which the half-life estimates are given in Table 5. According to the weakness of the γ branch of the then highly converted isomeric transition to the 13.5 keV $3/2^+$ state no such transition could be resolved in the present (n, γ) study, cf. Section 3.

6. *Conclusion*

The experimental knowledge about the level scheme of the nucleus ^{101}Mo has been considerably extended. In particular, new information about the spins and parities as well as the half-lives of the triplet of levels below 60 keV has been gained which plays a key role in the understanding of the structure of this isotope. An intensive study of the properties of the levels in terms of IBFM has been performed. A good fit to the data has been achieved when using an O(6)-like description of the core nucleus ^{100}Mo. No other parametrization has been found to be similarly successful.

Thus ^{101}Mo differs clearly from its $N = 59$ odd-mass isotones: Neither can its levels be reproduced with the assumption of a vibrational core as in the case of $^{97}Sr_{59}$[16], nor can the assumption[58] of a $J = j - 2, j - 1$ pattern as in ^{103}Ru[50] be upholded. This behaviour probably reflects the known structure transition in the even-even isotopes in this region where the lighter elements like Sr, Zr contain symmetric rotors while the heavier ones like Ru, Pd have a more complex structure. Surely, also the rapid change of the quasiparticle pattern[16] contributes. Further studies will be necessary to check, whether there is any shape coexistence with rotational patterns built on excited states as in ^{97}Sr[2,3].

Acknowledgements

The authors gratefully acknowledge the help of several colleagues in the operation of the different experiments and especially that by Dr. H. J. Scheerer in operating the Munich MP tandem.

References

1) F. Buchinger, E. B. Ramsay, R. E. Silverans, P. Lievens, E. Arnold, W. Neu, R. Neugart, K. Wendt, G. Ulm and the ISOLDE Collaboration, Z. Phys. **A**-Atomic Nuclei **327** (1987) 361;
2) G. Lhersonneau, B. Pfeiffer, K.-L. Kratz, H. Ohm and K. Sistemich, Z. Phys. **A**-Atomic Nuclei **330** (1988) 347;
3) G. Lhersonneau, K.-L. Kratz, H. Ohm, B. Pfeiffer and K. Sistemich, *Nuclear Structure of the Zirconium Region*, Proc. Intern. Workshop, Bad Honnef, April 24—28, 1988, eds. J. Eberth, R. A. Meyer, K. Sistemich (Springer-Verlag, 1988) p. 58;
4) J. Dubuc, G. Kairys, P. Larivière, S. Pilotte, W. Del Bianco and S. Monaro, Phys. Rev. **C37** (1988) 954;
5) B. B. Roy and D. C. Choundhury, Phys. Rev. **C12** (1975) 323;
6) K. Shizuma, H. Ahrens, J. P. Bocquet, N. Kaffrell, B. D. Kern, H. Lawin, R. A. Meyer, K. Sistemich, G. Tittel and N. Trautmann, Z. Phys. **A**-Atoms and Nuclei **315** (1984) 65;
7) Nuclear Data Sheets **45** (1985) 701;
8) H. Weigmann, S. Raman, J. A. Harvey, R. L. Macklin and G. G. Slaughter, Phys. Rev. **C20** (1979) 115;
9) E. E. Habib, private communication (1987) to R. A. Meyer;
10) B. Kardon, H. Seyfarth, P. Göttel and H. H. Güven, Proc. 2nd Int. Symp. Neutron Capture Gamma-Ray Spectroscopy, eds. K. Abrahams, F. Stecher-Rasmussen, P. van Assche (RCN Petten, The Netherlands, 1975), p. 544; Annual Report 1974, Institut für Kernphysik, KFA Jülich (1975) p. 123;
11) N. Kaffrell, G. Tittel, N. Trautmann, H. Ahrens, J. P. Bocquet, B. Pfeiffer, E. Monnand and F. Schussler, Jahresbericht 1975, Institut für Kernchemie, Universität Mainz (1976) p. 63;
12) W.-D. Lauppe, T. A. Khan, H. Lawin, G. Sadler, H. A. Selič, K. Sistemich and W. Tenten, Annual Report 1976, Institut für Kernphysik, KFA Jülich (1977) p. 44;

13) P. Glässel, E. Huenges, P. Maier-Komor, H. Rösler, H.-J. Scheerer and H. Vonach, Jahresbericht 1975, Beschleunigerlaboratorium der Universität und der Technischen Universität München, p. 88;
14) H. Seyfarth, H. H. Güven, B. Kardon, W. D. Lauppe, G. Lhersonneau, K. Sistemich, S. Brant, N. Kaffrell, P. Maier-Komor, H. K. Vonach, V. Paar, D. Vorkapić and R. A. Meyer, Z. Phys. **A**-Atomic Nuclei, to be published;
15) K. Sistemich, K. Kawade, H. Lawin, G. Lhersonneau, H. Ohm, U. Paffrath, V. Lopac, S. Brant and V. Paar, Z. Phys. **A**-Atomic Nuclei **325** (1986) 139; S. Brant, K. Sistemich, V. Paar and G. Lhersonneau, Z. Phys. **A**-Atomic Nuclei **330** (1988) 365; S. Brant, G. Lhersonneau, V. Paar and K. Sistemich, Z. Phys. **A**-Atomic Nuclei **333** (1989) 1;
16) S. Brant, K. Sistemich, H. Seyfarth, H. Ohm, M. L. Stolzenwald, V. Paar, D. Vretenar, D. Vorkapić, V. Lopac, R. A. Meyer, G. Lhersonneau, K.-L. Kratz and B. Pfeiffer, as Ref. 3, p. 199;
17) S. Brant, G. Lhersonneau, M. L. Stolzenwald, K. Sistemich and V. Paar, Z. Phys. **A**-Atomic Nuclei **329** (1988) 301;
18) E. Moll, H. Schrader, G. Siegert, M. Asghar, J. P. Bocquet, G. Bailleul, J. P. Gautheron, J. Greif, G. I. Crawford, C. Chauvin, H. Ewald, H. Wollnik, P. Armbruster, G. Fiebig, H. Lawin and K. Sistemich, Nucl. Instrum. Methods **123** (1975) 615;
19) S. F. Mughabghab, M. Divadeenam and N. E. Holden, *Neutron Cross Sections* (Academic Press, New York, 1981) Vol. 1;
20) W. Delang, P. Göttel and H. Seyfarth, Nucl. Instrum. Methods **99** (1972) 13;
21) H. Seyfarth, S. Brant, P. Göttel, V. Paar, D. Vorkapić and D. Vretenar, Z. Phys. **A**-Atomic Nuclei **330** (1988) 141;
22) R. Weishaupt and D. Rabenstein, Z. Physik **251** (1972) 105;
23) H. H. Schmidt, P. Hungerford, H. Daniel, T. von Egidy, S. A. Kerr, R. Brissot, G. Barreau, H. G. Börner, C. Hofmeyr and K. P. Lieb, Phys. Rev. **C25** (1982) 2888;
24) H. Seyfarth, A. M. Hassan, B. Hrastnik, P. Göttel and W. Delang, Nucl. Instrum. Methods **105** (1972) 301;
25) C. M. Lederer, V. S. Shirley (eds.), *Table of Isotopes* (John Wiley Sons, New York, 1978);
26) C. van der Leun, P. de Wit and C. Alderliesten, *Neutron-Capture Gamma-Ray Spectroscopy and Related Topics 1981* eds. T. v. Egidy, F. Gönnenwein and B. Maier (Conf. Ser. No. 62, The Institute of Physics, Bristol and London, 1982) p. 548;
27) E. K. Warburton, D. E. Alburger and D. J. Millener, Phys. Rev. **C22** (1980) 2330;
28) E. R. Cohen and A. H. Wapstra, Nucl. Instrum. Meth. **211** (1983) 153;
29) R. C. Greenwood and R. E. Chrien, Phys. Rev. **C24** (1980) 498;
30) T. J. Kennett, W. V. Prestwich, R. J. Tervo and J. S. Tsai, Nucl. Instrum. Meth. **215** (1983) 159;
31) G. E. Thomas, D. E. Blatchley and L. M. Bollinger, Nucl. Instrum. Meth. **56** (1967) 325;
32) G. D. Loper and G. E. Thomas, Nucl. Instrum. Meth. **105** (1972) 453;
33) P. Maier-Komor, P. Glässel, E. Huenges, H. Rösler, H. J. Scheerer and H. K. Vonach, Z. Phys. **A**-Atoms and Nuclei **278** (1976) 327;
34) S. A. Hjorth and B. L. Cohen, Phys. Rev. **B135** (1964) 920;
35) W. L. Sievers, D. A. Close, C. J. Umbarger, R. C. Bearse and F. W. Posser, Jr., Phys. Rev. **C6** (1972) 1001;
36) W. Booth, S. M. Dalgliesh, K. C. McLean, R. N. Glover and F. R. Hudson, Phys. Lett. **30B** (1969) 335;
37) T. von Egidy, private communication to H. Seyfarth;
38) T. von Egidy, *Neutron Capture Gamma-Ray Spectroscopy*, ed. N. Ryde (Proceedings Series, IAEA, Vienna, 1969) p. 541;
39) Gulf General Atomic report GA-10248 (1970);
40) E. G. Kessler, Jr., R. D. Deslattes, A. Henins and W. C. Sauder, Phys. Rev. Lett. **40** (1978) 171;
41) E. G. Kessler, Jr., R. D. Deslattes, D. Girard, W. Schwitz, L. Jacobs and O. Renner, Phys. Rev. **A26** (1982) 2696;
42) F. Rösel, H. M. Fries, K. Alder and H. C. Pauli, Atomic Data and Nuclear Data Tables **21** (1978);
43) A. Arima and F. Iachello, Ann. Phys. **99** (1976) 253;
44) D. Janssen, R. V. Jolos and F. Dönau, Nucl. Phys. **A224** (1974) 93;
45) V. Paar, S. Brant, L. F. Canto, G. Leander and M. Vouk, Nucl. Phys. **A378** (1982) 41; V. Paar, Verhandl. der Deutschen Physikalischen Gesellschaft **3** (1979) 683;
46) F. Iachello and O. Scholten, Phys. Rev. Lett. **43** (1979) 679;
47) Y. Tokunaga, H. Seyfarth, O. W. B. Schult, S. Brant, V. Paar, D. Vretenar, H.G.Börner, G. Barreau, H. Faust, Ch. Hofmeyr and K. Schreckenbach, Nucl. Phys. **A430** (1984) 269;

48) S. Brant, V. Paar, D. Vorkapić, D. Vretenar, V. Lopac and R. A. Meyer, Fizika (Yugoslavia) **19** (1987) 453;
49) R. A. Meyer, N. Kusnezov, S. V. Jackson, S. Brant and V. Paar, submitted for publication to Phys. Rev. C;
50) H. Seyfarth, K. Schreckenbach, S. Brant and V. Paar, Annual Report 1984, Institut für Kernphysik, KFA Jülich, F. R. Germany, Report Jül-Spez-305 (1985) p. 99, to be published;
51) O. Scholten, Thesis, University of Groningen (1980);
52) V. Paar, Nucl. Phys. **A211** (1973) 29;
53) K. Heyde and V. Paar, Phys. Lett. **179B** (1986) 1;
54) R. C. Diehl, B. L. Cohen, R. A. Moyer and L. H. Goldman, Phys. Rev. **C1** (1970) 2132;
55) M. Sambataro and G. Molnár, Nucl. Phys. **A376** (1982) 201;
56) R. A. Meyer et al., to be published;
57) V. Paar and S. Brant, Phys. Lett. **74B** (1978) 297; Nucl. Phys. **A303** (1978) 606;
58) R. A. Meyer and K. Sistemich, Proc. 7th Int. Conf. on Atomic Masses and Fundamental Constants, AMCO-7, Darmstadt, September 3—7, 1984, ed. O. Klepper (Publ. TH Darmstadt, 1984) p. 523.

STRUKTURA NISKOLEŽEĆIH STANJA JEZGRE ^{101}Mo

HELMUTH SEYFARTH, HASAN H. GÜVEN, BELA KARDON, GÉRARD LHERSONNEAU, KORNEL SISTEMICH i SLOBODAN BRANT

Institut für Kernphysik, KFA Jülich, Jülich, F. R. Germany

NORBERT KAFFRELL

Institut für Kernchemie, Johannes Gutenberg-Universität Mainz, Mainz, F. R. Germany

PETER MAIER-KOMOR

Physik-Department, Technische Universität München, Garching, F. R. Germany

HELBERT K. VONACH

Institut für Radiumforschung und Kernphysik der Universität Wien, Wien, Austria

VLADIMIR PAAR i DRAŽEN VORKAPIĆ

Prirodoslovno-matematički fakultet, University of Zagreb, Zagreb, Yugoslavia

RICHARD A. MEYER

Nuclear Physics Division, U. S. Department of Energy Washington D. C. i *Lawrence Livermore National Laboratory, Livermore, California, USA*

UDK 539.14

Originalni znanstveni rad

Proučavana su pobuđena stanja ^{101}Mo s energijama do 1447 keV. Provedeni su računi u bozonsko-fermionskom modelu IBFM/PTQM uzimajući u obzir prelazni karakter sredice ^{100}Mo.